

# Hunting ewinos and a light scalar of $Z_3$ -NMSSM with a bino-like dark matter in top squark decays at the LHC

Asesh Krishna Datta,<sup>a</sup> Monoranjan Guchait,<sup>b</sup> Arnab Roy<sup>b</sup> and Subhojit Roy<sup>a,c</sup>

<sup>a</sup>*Harish-Chandra Research Institute, A CI of Homi Bhabha National Institute, Chhatnag Road, Jhansi, Prayagraj (Allahabad) 211019, India*

<sup>b</sup>*Department of High Energy Physics, Tata Institute of Fundamental Research, Homi Bhabha Road, Mumbai-400005, India*

<sup>c</sup>*Regional Centre for Accelerator-based Particle Physics, Harish-Chandra Research Institute, Chhatnag Road, Jhansi, Prayagraj (Allahabad) 211019, India*

*E-mail:* [asesh@hri.res.in](mailto:asesh@hri.res.in), [guchait@tifr.res.in](mailto:guchait@tifr.res.in), [arnab.roy@tifr.res.in](mailto:arnab.roy@tifr.res.in), [subhojitroy@hri.res.in](mailto:subhojitroy@hri.res.in)

**ABSTRACT:** We explore a possible signal of the presence of relatively light electroweakinos (ewinos) and a singlet-like scalar ( $a_s$ ) of the  $Z_3$ -symmetric Next-to-Minimal Supersymmetric Standard Model ( $Z_3$ -NMSSM) in the cascade decays of not so heavy top squarks ( $m_{\tilde{t}_1} \lesssim 1.5$  TeV) that may be produced in pairs at the Large Hadron Collider LHC. We work in a scenario where the lightest (next-to-lightest) SUSY particle is bino (singlino)-like with its mass below 100 GeV and is mildly tempered with higgsino and singlino admixtures. The singlet-like scalar provides an annihilation funnel for the bino-like states such that the latter could act as a viable dark matter candidate, unlike what is now highly constrained in the MSSM. We consider a pair of immediately heavier neutralinos and the lighter chargino which all are higgsino-like with masses in the range  $\sim 0.5$ –1 TeV and are still compatible with all experimental constraints. While these states may not be accessible in their direct searches at the LHC in our present scenario, such ewinos could still be traced in the decays of the top squarks of the above-mentioned kind. We consider the signal final state  $1\ell(e, \mu) + (\geq 1) a_s(b\bar{b}) + (\geq 1) h_{\text{SM}}(b\bar{b}) + \geq 4 \text{ jets} + \cancel{E}_T$  at the LHC. We find that while a usual cut-based analysis (CBA) of LHC data worth  $300 \text{ fb}^{-1}$  would be unable to discover such excitations, a multivariate analysis (MVA) can be reasonably sensitive to higgsino-like ewinos having masses  $\gtrsim 650$  GeV when  $m_{\tilde{t}_1} \gtrsim 1$  TeV. On the other hand, with  $3000 \text{ fb}^{-1}$  of data, these masses become accessible in a CBA while even an MVA on such a data set is unlikely to find these ewinos with masses around 1 TeV when  $m_{\tilde{t}_1}$  hits  $\sim 1.5$  TeV.

**KEYWORDS:** Beyond Standard Model, Supersymmetry Phenomenology

---

## Contents

<b>1</b>	<b>Introduction</b>	<b>1</b>
<b>2</b>	<b>The theoretical framework: the <math>Z_3</math>-NMSSM</b>	<b>5</b>
2.1	The Higgs sector	5
2.2	The ewino sector	7
2.3	The top and bottom squark sector	8
2.4	Interactions of the ewinos with $\tilde{t}_1$ , the Higgs and the gauge bosons	9
2.4.1	Interactions of the ewinos with $\tilde{t}_1$	9
2.4.2	Interactions of the ewinos with the Higgs and the gauge bosons	10
<b>3</b>	<b>The motivated region of the <math>Z_3</math>-NMSSM parameter space</b>	<b>11</b>
<b>4</b>	<b>The setup of the analysis</b>	<b>15</b>
4.1	The spectra and the constraints	15
4.2	The benchmark scenarios	16
4.3	An NMSSM-specific signal and the SM backgrounds	20
4.4	The simulation framework	20
4.5	Object reconstruction	21
<b>5</b>	<b>Results</b>	<b>22</b>
5.1	The cut-based analysis	22
5.2	A multivariate analysis	27
<b>6</b>	<b>Summary and outlook</b>	<b>31</b>
<b>7</b>	<b>Acknowledgments</b>	<b>33</b>

---

## 1 Introduction

The Next-to-Minimal Supersymmetric Standard Model (NMSSM) was originally motivated as a solution to the well-known ‘ $\mu$ ’-problem [1] that plagues the minimal supersymmetric (SUSY) extension of the Standard Model (SM), i.e., the MSSM, via the introduction of a gauge singlet superfield. The NMSSM is known for long to possess a non-trivial phenomenology by virtue of its richer scalar and electroweakino (ewinos, i.e., charginos and neutralinos) sectors in the presence of singlet degrees of freedom which can be rather light and have characteristic interactions.

Incidentally, the scenario has attracted a renewed attention post the discovery of the SM-like Higgs boson ( $h_{\text{SM}}$ ) with a mass ( $m_{h_{\text{SM}}}$ ) around 125 GeV [2, 3] at the Large Hadron

Collider (LHC). This is since while in the MSSM attaining such a mass requires a large radiative correction and hence much heavier top squarks ( $\tilde{t}_{1,2}$ ; running in the loops) thus rendering the scenario somewhat ‘unnatural’, the NMSSM provides a more ‘natural’ setup as it finds new tree-level contributions to  $m_{h_{\text{SM}}}$  and hence banks less on too heavy top squarks.

Naturally, various phenomenological aspects of the NMSSM, in particular, of its  $Z_3$ -symmetric incarnation ( $Z_3$ -NMSSM), have since been either meticulously revisited or have been explored freshly. These not only include studies in the usual fronts like the colliders and the dark matter (DM) but, of recent, also have opened up to its cosmological implications pertaining to the stability of the vacuum [4, 5], phase transitions in the early Universe [6–8], electroweak baryogenesis [9], etc. Such studies have explored the deep connections among these fronts, the common thread being the scalar and the ewino sectors, now augmented by new gauge-singlet states (two singlet scalars and a singlet fermion, i.e., the singlino) when compared to the MSSM case.

In this work, a specific choice is made over the neutralino spectrum where the lightest SUSY particle (LSP) is bino-like (i.e.,  $\chi_1^0 \approx \tilde{B}$ ), the next-to-LSP (NLSP) is singlino-like (i.e.,  $\chi_2^0 \approx \tilde{S}$ ) while the two immediately heavier neutralinos and the lighter chargino ( $\chi_{3,4}^0, \chi_1^\pm \approx \tilde{H}$ ) are higgsino-like with very similar masses. The wino-like states ( $\chi_5^0$  and  $\chi_2^\pm$ ) are taken to be much heavier and hence those are effectively decoupled from the phenomenology we discuss in this work.

Such a hierarchy of ewinos, in particular, with a light LSP (NLSP) which is bino-like (singlino-like), has recently been highlighted [10] to open up the possibility of having a bino-like DM in the  $Z_3$ -NMSSM, something that is highly disfavoured in the MSSM given the current experimental constraints from both the collider and the cosmology fronts. In the  $Z_3$ -NMSSM, this is facilitated by a light singlet-like  $CP$ -even scalar,  $h_s$ , (which necessarily accompanies a relatively light singlino-like state [10–16]), and/or a light  $CP$ -odd scalar,  $a_s$ , when these provide efficient funnels for the mutual annihilation of the bino-like DM, which is tempered with small higgsino and singlino admixtures. This is possible without inviting a conflict with various bounds obtained from the DM direct detection (DMDD) experiments (of both spin-independent (SI) and spin-dependent (SD) kinds) thanks to the occurrence of new ‘blind spots’ [10]. However, in this regard, the tempering of the bino-like LSP with the higgsino admixtures has to, otherwise, maintain a delicate balance. Such a situation, to a good extent, can be ameliorated by pushing  $\mu_{\text{eff}}$  up, optimally, without requiring it to be just that large when the DM annihilation rate starts suffering, thus leaving too large a relic. Such a spectrum of ewinos and light scalar(s) has been shown [10] to bear a further theoretical motivation as this can trigger a strong first-order electroweak phase transition (SFOEWPT) in the early Universe. This could not only set the stage for a successful electroweak baryogenesis (EWBG) that might explain the experimentally measured baryon asymmetry in the present day Universe, but also could be a potential source of detectable gravitational waves (GWs).

For such a spectrum, direct productions of the NLSP, which is singlino-dominated, would be naturally suppressed (because of its singlet nature) even though it could be reasonably light. Hence this might escape searches at the LHC. On the other hand, the higgsino-

like states can stay relatively light (thus aiding ‘naturalness’) and still remain insensitive to searches in their direct productions. This is because their cascades could now involve singlet-like scalar(s) and the singlino-like neutralino.

It is to be noted that the most sensitive of searches for relatively light ewinos in their direct productions at the 13 TeV LHC involve multi-lepton plus multi-jet final states accompanied by missing transverse energy (MET,  $\cancel{E}_T$ ). In particular, the strongest ever lower bounds on their masses come from the search in the rather clean  $3\ell + \cancel{E}_T$  final state arising in the direct production of wino-like  $\chi_1^\pm \chi_2^0$  cascading via the  $WZ$ -mode, where both  $W^\pm$ - and  $Z$ -bosons decay leptonically [17–21] or from a search in the final state  $2\ell + 2\text{-jet} + \cancel{E}_T$ , where  $W^\pm$  decays hadronically [17–19] or in the  $WH$ -mode [22], by analyzing the final state  $1\ell + 2b\text{-jet} + \cancel{E}_T$ , where the  $b$ -jets originate in the decay of  $h_{\text{SM}}$ . In contrast, in the  $Z_3$ -NMSSM scenario we consider in this work, the concerned neutralinos are higgsino-like (instead of being wino-like) and the corresponding mass bounds are already expected to be relaxed given their smaller combined direct production cross section at the LHC. On top of that, as mentioned above, their possible cascades involving singlet-like scalars and/or the singlino could further erode their sensitivities to current searches at the LHC.

At this point, the theoretical possibility of having relatively light top squarks could bring such states into the mix in a rather involved way. As such, stringent lower bounds on the mass of the lighter top squark ( $m_{\tilde{t}_1}$ ), as obtained by the LHC experiments within the MSSM framework, could still hold in an NMSSM scenario as long as  $\tilde{t}_1$  decays in ways similar to those in the MSSM. However, in the presence of a light singlino-like neutralino and light singlet-like scalars, the pattern of cascade decays of  $\tilde{t}_1$ , via heavier ewinos, could get altered in an essential way. This could relax the lower bounds on  $m_{\tilde{t}_1}$  as reported by the LHC experiments. Such modifications can be triggered by the altered decay patterns of the somewhat heavier ewinos, produced in the decays of  $\tilde{t}_1$ , to their lighter cousins which are now accompanied by light singlet-like scalar(s). Note that, as discussed earlier, in the first place, such NMSSM-specific cascades of the ewinos could lead to relaxed lower bounds on their own masses as obtained by the LHC experiments within the MSSM framework. However, now, in the presence of a relatively light  $\tilde{t}_1$  once the reach for the ewinos in their direct (electroweak) productions at the LHC saturates, the same can be extended by hunting them down in the cascades of  $\tilde{t}_1$  that would be produced strongly at the LHC [23].

To be specific, we choose to work with a bino-like LSP with its mass well below 100 GeV and a singlino-like NLSP not much heavier than 100 GeV while the higgsino-like neutralinos and the higgsino-like lighter chargino have their masses in the ballpark of 500 GeV or above, up to about 1 TeV. Such a choice for the LSP mass, in the presence of an NLSP and the higgsino-like states of the chosen kinds, is motivated by the fact that these, when acting in tandem, have been demonstrated [10] to relax the DM direct detection constraints where those tend to get increasingly stronger. Also, we consider  $m_{\tilde{t}_1}$  over the range  $\sim 800$  GeV – 1.5 TeV for our analysis at the 13 TeV LHC.<sup>1</sup> Note that such spectra are expected to evade

---

<sup>1</sup>We carry out our analyses by considering a 13 TeV LHC run that eventually would have collected data worth 3000 fb<sup>-1</sup>. Results obtained with this consideration are unlikely to be affected in any essential way in the upcoming runs of the LHC with a slightly increased centre of mass energy.

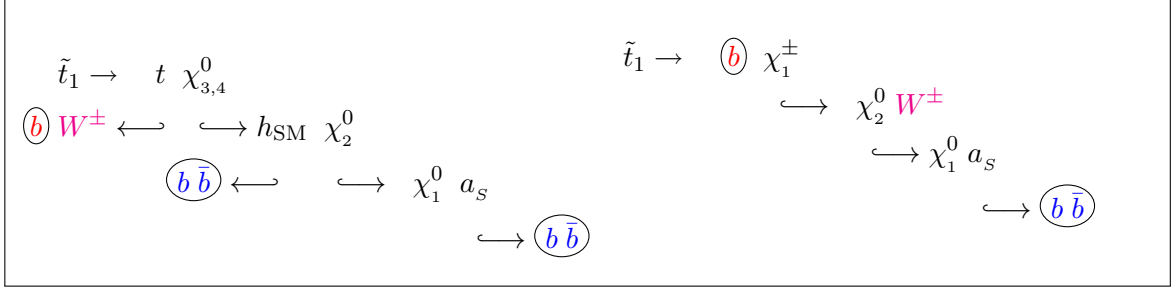


**Figure 1.** Possible cascades of  $\tilde{t}_1$  explored in this work that lead to the chosen signal final state  $1\ell(e, \mu) + (\geq 1)a_s(b\bar{b}) + (\geq 1)h_{\text{SM}}(b\bar{b}) + \geq 4\text{jets} + \cancel{E}_T$ .

lower bounds on the involved masses from the LHC experiments, are compatible with the constraints from the DM sector and are also able to trigger SFOEWPT leading to EWBG in the early Universe [8]. Possible cascades of  $\tilde{t}_1$  that we explore in this work (and which lead to our chosen signal final state) are schematically shown in the rectangular box.

As can be seen, for such a spectrum, the ensuing cascades of  $\tilde{t}_1$  might produce  $h_{\text{SM}}$  when  $\chi_{3,4}^0$  decay to  $\chi_{1,2}^0$ , of which their decays to the singlino-like  $\chi_2^0$  are of special interest. This is not only because a singlet-like scalar,  $a_s$ , accompanies the same but also since, over the region of the parameter space that we are interested in, such decays of  $\chi_{3,4}^0$  are favored. Hence, as may be expected, the final states are going to be rich in bottom quark jets, which will come from the decays of  $h_{\text{SM}}$ ,  $a_s$  and the top quarks arising from the cascades of  $\tilde{t}_1$  and/or from  $\tilde{t}_1$ 's direct decay to a bottom quark with an accompanying lighter chargino,  $\chi_1^\pm$ . Hence the specific signal final state that we study in this work, in the context of the high luminosity run of the LHC (HL-LHC), is 1 lepton + 4  $b$ -jets +  $\geq 4$  jets +  $\cancel{E}_T$  in which the two pairs of  $b$ -jets are required to get reconstructed to  $h_{\text{SM}}$  and  $a_s$ .

A few benchmark points are then picked up based on the mass and the dominant chiral content of  $\tilde{t}_1$ . We perform both a cut-based study and a MultiVariate Analysis (MVA) [24] using the Boosted Decision Tree (BDT) [25] and compare their performances in deciphering the signal from the background. The sensitivities of the LHC to the proposed signal are further compared for accumulated luminosities of  $300 \text{ fb}^{-1}$  and  $3000 \text{ fb}^{-1}$ .

The paper is organized as follows. In section 2 we discuss the theoretical framework of the  $Z_3$ -NMSSM by outlining the scalar (Higgs), the ewino and the top squark sectors and highlight how the masses of various excitations from these sectors and their mutual interactions, that are so crucial for the phenomenology we discuss, depending on the underlying parameters of the theory. Section 3 is devoted to establishing the region of the  $Z_3$ -NMSSM parameter space that is particularly interesting for our present purpose. The setup of our analysis is presented in section 4 which includes discussions of various constraints that we consider, both theoretical and experimental, the descriptions of the  $Z_3$ -NMSSM-specific signal that we are interested in and the relevant backgrounds as well as the strategy of reconstructing the final state objects. Section 5 discusses in detail the results of our simulations by comparing the significances and/or reach of the  $Z_3$ -NMSSM-specific signal that we propose over the SM background at the 13 TeV LHC as obtained via a usual cut-based analysis and via a

multivariate approach. In section 6 we conclude.

## 2 The theoretical framework: the $Z_3$ -NMSSM

The most general  $Z_3$ -NMSSM superpotential, with conserved  $R$ -parity, is given by [26]

$$\mathcal{W} = \mathcal{W}_{\text{MSSM}}|_{\mu=0} + \lambda \hat{S} \hat{H}_u \cdot \hat{H}_d + \frac{\kappa}{3} \hat{S}^3, \quad (2.1)$$

where  $\mathcal{W}_{\text{MSSM}}|_{\mu=0}$  represents the MSSM superpotential without the higgsino mass term (known as the  $\mu$ -term),  $\hat{H}_u, \hat{H}_d$  and  $\hat{S}$  are the  $SU(2)$  Higgs doublet superfields and the gauge singlet superfield, respectively, and ‘ $\lambda$ ’ and ‘ $\kappa$ ’ are dimensionless coupling constants. The addition of a singlet superfield  $\hat{S}$  to the MSSM helps solve the so-called  $\mu$ -problem when its scalar component develops a non-zero vacuum expectation value ( $v_{\text{ev}}$ )  $v_s$  thereby generating an effective  $\mu$ -term dynamically which is given by  $\mu_{\text{eff}} = \lambda v_s$  and can be obtained from the second term on the right-hand side of equation 2.1. The corresponding soft SUSY-breaking Lagrangian is given by

$$-\mathcal{L}^{(\text{soft})} = -\mathcal{L}_{\text{MSSM}}^{(\text{soft})}|_{B\mu=0} + m_S^2 |S|^2 + (\lambda A_\lambda S H_u \cdot H_d + \frac{\kappa}{3} A_\kappa S^3 + \text{h.c.}), \quad (2.2)$$

where ‘ $B$ ’ is the soft SUSY-breaking bilinear parameter of the MSSM associated with the Higgsino mass term,  $m_S$  is the soft SUSY-breaking mass of the singlet scalar field ‘ $S$ ’ while  $A_\lambda$  and  $A_\kappa$  are the NMSSM-specific trilinear soft couplings, all of which are of mass dimension one. In this study, we do not consider  $CP$ -violating entries that might be present in the scalar and/or the ewino sectors. Hence all the Lagrangian parameters are taken to be real. In the upcoming subsections, we briefly discuss the structures of the Higgs, the ewino and the top squark sectors and the interactions involving them which are instrumental in the phenomenology we discuss in the rest of this work.

### 2.1 The Higgs sector

The  $Z_3$ -NMSSM has the following tree-level Higgs (scalar) potential:

$$V_{\text{tree}}^{\text{NMSSM}} = V_F + V_D + V_{\text{soft}}, \quad (2.3a)$$

where contributions from the  $F$ - and  $D$ -terms as well as those from the soft SUSY-breaking terms, as represented by the variables  $V_F$ ,  $V_D$  and  $V_{\text{soft}}$ , respectively, are given by

$$V_F = |\lambda S|^2 (|H_u|^2 + |H_d|^2) + |\lambda H_u \cdot H_d + \kappa S^2|^2, \quad (2.3b)$$

$$V_D = \frac{1}{8} g^2 (|H_u|^2 - |H_d|^2)^2 + \frac{1}{2} g_2^2 |H_u^\dagger H_d|^2, \quad (2.3c)$$

$$V_{\text{soft}} = m_{H_u}^2 |H_u|^2 + m_{H_d}^2 |H_d|^2 + m_S^2 |S|^2 + (\lambda A_\lambda S H_u \cdot H_d + \frac{\kappa}{3} A_\kappa S^3 + \text{h.c.}), \quad (2.3d)$$

where  $g^2 = (g_1^2 + g_2^2)/2$  and  $g_1$  and  $g_2$  are the  $U(1)$  and the  $SU(2)$  gauge couplings, respectively. The complex Higgs fields can be then expressed as

$$H_u = \begin{pmatrix} H_u^+ \\ v_u + \frac{1}{\sqrt{2}} (H_{uR} + i H_{uI}) \end{pmatrix}, \quad H_d = \begin{pmatrix} v_d + \frac{1}{\sqrt{2}} (H_{dR} + i H_{dI}) \\ H_d^- \end{pmatrix}, \quad S = v_s + \frac{S_R + i S_I}{\sqrt{2}}, \quad (2.4)$$

where suffixes ‘ $R$ ’ and ‘ $I$ ’ stand for the  $CP$ -even and the  $CP$ -odd components of the complex fields and  $v_u, v_d$  and  $v_s$  are the  $vevs$  of the  $CP$ -even components of the neutral scalar fields with  $\sqrt{v_u^2 + v_d^2} = v \simeq 174$  GeV,  $\tan \beta = v_u/v_d$  and  $\mu_{\text{eff}} = \lambda v_s$  (as mentioned earlier). Thus, the symmetric ( $3 \times 3$ ) mass-squared matrix for the  $CP$ -even Higgs bosons of the  $Z_3$ -symmetric NMSSM, in the basis  $H_{jR} = \{H_{dR}, H_{uR}, S_R\}$ , is given by [26]

$$\mathcal{M}_S^2 = \begin{pmatrix} g^2 v_d^2 + \mu_{\text{eff}} B_{\text{eff}} \tan \beta & (2\lambda^2 - g^2) v_u v_d - \mu_{\text{eff}} B_{\text{eff}} & \lambda(2\mu_{\text{eff}} v_d - (B_{\text{eff}} + \kappa v_s) v_u) \\ \dots & g^2 v_u^2 + \mu_{\text{eff}} B_{\text{eff}} / \tan \beta & \lambda(2\mu_{\text{eff}} v_u - (B_{\text{eff}} + \kappa v_s) v_d) \\ \dots & \dots & \lambda A_\lambda \frac{v_u v_d}{v_s} + \kappa v_s (A_\kappa + 4\kappa v_s) \end{pmatrix}, \quad (2.5)$$

where  $B_{\text{eff}} = A_\lambda + \kappa v_s$  is the effective ‘ $B$ ’ term of the  $Z_3$ -NMSSM. The resulting  $CP$ -even (scalar) mass eigenstates are given by

$$h_i = S_{ij} H_{jR}, \quad \text{with } i, j = 1, 2, 3, \quad (2.6)$$

where the matrix ‘ $S$ ’ diagonalizes  $\mathcal{M}_S^2$ . In a rotated basis  $(\hat{h}, \hat{H}, \hat{s})$  [27, 28], where  $\hat{h} = H_{dR} \cos \beta + H_{uR} \sin \beta$ ,  $\hat{H} = H_{dR} \sin \beta - H_{uR} \cos \beta$  and  $\hat{s} = S_R$ , the  $CP$ -even state  $\hat{h}$  ( $\hat{H}$ ) now mimics the SM Higgs (MSSM (doublet)-like heavier  $CP$ -even Higgs boson, ‘ $H$ ’) field. In this basis, the  $CP$ -even scalar mass eigenstates possess the following generic admixtures:

$$h_i = E_{h_i \hat{h}} \hat{h} + E_{h_i \hat{H}} \hat{H} + E_{h_i \hat{s}} \hat{s}, \quad (2.7)$$

where the matrix  $E_{ab}$  diagonalizes the mass-squared matrix for the  $CP$ -even scalars in the rotated basis. On the other hand, the symmetric ( $3 \times 3$ ) mass-squared matrix for the  $CP$ -odd scalars in the basis  $H_{jI} = \{H_{dI}, H_{uI}, S_I\}$  is given by [26]

$$\mathcal{M}_P^2 = \begin{pmatrix} \mu_{\text{eff}} B_{\text{eff}} \tan \beta & \mu_{\text{eff}} B_{\text{eff}} & \lambda v_u (A_\lambda - 2\kappa v_s) \\ \dots & \mu_{\text{eff}} B_{\text{eff}} / \tan \beta & \lambda v_d (A_\lambda - 2\kappa v_s) \\ \dots & \dots & \lambda (B_{\text{eff}} + 3\kappa v_s) \frac{v_u v_d}{v_s} - 3\kappa A_\kappa v_s \end{pmatrix}. \quad (2.8)$$

For  $\mathcal{M}_P^2$ , a similar rotation in the basis of the doublet states  $H_{dI}$  and  $H_{uI}$  would, as can be expected, project out the massless Nambu-Goldstone mode which can be dropped. The (doublet)-like  $CP$ -odd (pseudoscalar) Higgs boson of the MSSM can be identified with  $A = \cos \beta H_{uI} + \sin \beta H_{dI}$  and in the basis  $\{A, S_I\}$ , the symmetric ( $2 \times 2$ ) mass-squared matrix for the  $CP$ -odd scalars of the  $Z_3$ -NMSSM gets reduced to

$$\mathcal{M}_P^2 = \begin{pmatrix} m_A^2 & \lambda (A_\lambda - 2\kappa v_s) v \\ \lambda (A_\lambda - 2\kappa v_s) v & \lambda (A_\lambda + 4\kappa v_s) \frac{v_u v_d}{v_s} - 3\kappa A_\kappa v_s \end{pmatrix}, \quad (2.9)$$

where, along the lines of the MSSM,  $m_A^2 = 2\mu_{\text{eff}} B_{\text{eff}} / \sin 2\beta$ . The  $CP$ -odd (pseudoscalar  $a_k$ ) mass eigenstates are then given by

$$a_k = \mathcal{O}_{kA} A + \mathcal{O}_{kS_I} S_I, \quad \text{with } k = 1, 2, \quad (2.10)$$

where the matrix ‘ $\mathcal{O}$ ’ diagonalizes  $\mathcal{M}_P^2$ .



For a negligible singlet-doublet ( $\{H_{dR}-H_{uR}\}-S_R$ ) mixing, the squared mass (at the tree-level) of the singlet-like  $CP$ -even physical state can be approximated as

$$m_{h_S}^2 \approx \mathcal{M}_{S,33}^2 = \lambda A_\lambda \frac{v_u v_d}{v_S} + \kappa v_S (A_\kappa + 4\kappa v_S). \quad (2.11)$$

For  $m_A \gg m_Z$  (i.e., in the so-called decoupling limit), the masses of the heavier of the MSSM (doublet)-like  $CP$ -even Higgs boson ( $H$ ) and the charged Higgs bosons ( $H^\pm$ ) approach  $m_A$ , i.e.,  $m_H \approx m_{H^\pm} \approx m_A$ . On the other hand, the squared mass of the lighter one mimicking  $h_{\text{SM}}$  is given by [29]

$$m_{h_{\text{SM}}}^2 = m_Z^2 \cos^2 2\beta + \lambda^2 v^2 \sin^2 2\beta + \Delta_{\text{mix}} + \Delta_{\text{rad. corr.}}, \quad (2.12)$$

where the first term on the right-hand side is the tree-level MSSM contribution, while the second and the third terms are new tree-level contributions from the NMSSM.  $\Delta_{\text{mix}}$  has its origin in a possible singlet-doublet mixing and in the limit of a weak mixing,  $\Delta_{\text{mix}}$  is given by [29]

$$\Delta_{\text{mix}} = \frac{4\lambda^2 v_S^2 v^2 (\lambda - \kappa \sin 2\beta)^2}{\tilde{m}_h^2 - m_{ss}^2}, \quad (2.13)$$

where  $m_{ss}^2 = \kappa v_S (A_\kappa + 4\kappa v_S)$  and  $\tilde{m}_h^2 = m_{h_{\text{SM}}}^2 - \Delta_{\text{mix}}$ . For  $v_S \gg v_u, v_d$ , one finds  $m_{ss}^2 \approx \mathcal{M}_{S,33}^2 \approx m_{h_S}^2$ . The term  $\Delta_{\text{rad. corr.}}$  captures the dominant radiative corrections in the MSSM at one-loop level (with the top quark and the top squarks running in the loops) to  $m_{h_{\text{SM}}}^2$  and is given by [30, 31]

$$\Delta_{\text{rad. corr.}}^{1\text{-loop}} \simeq \frac{3m_t^4}{4\pi^2 v^2 \sin^2 \beta} \left[ 2 \log \frac{M_S}{m_t} + \frac{X_t^2}{M_S^2} \left( 1 - \frac{X_t^2}{12M_S^2} \right) \right], \quad (2.14)$$

where  $m_t$  denotes the mass of the SM top quark,  $M_S = \sqrt{m_{\tilde{t}_1} m_{\tilde{t}_2}}$ ,  $m_{\tilde{t}_1(\tilde{t}_2)}$  being the mass of the lighter (heavier) physical top squark state and  $X_t = A_t - \mu_{\text{eff}} \cot \beta$ ,  $A_t$  being the soft trilinear coupling for the top sector.

As for the singlet  $CP$ -odd scalar,  $a_s$ , its squared mass, up to a small mixing with the doublet-like  $CP$ -odd state, is given by

$$m_{a_s}^2 \approx \mathcal{M}_{P,22}^2 = \lambda(A_\lambda + 4\kappa v_S) \frac{v_u v_d}{v_S} - 3\kappa A_\kappa v_S. \quad (2.15)$$

The expressions for  $m_{h_{\text{SM}}}$ ,  $m_{H,A}$ ,  $m_{h_S}$  and  $m_{a_s}$  presented above reveal their nontrivial dependencies on various input parameters of the  $Z_3$ -NMSSM and point to characteristic correlations among these masses. Together, these could crucially govern the collective phenomenology involving these states at both colliders and at the DM/cosmology front.

## 2.2 The ewino sector

The neutralino sector of the  $Z_3$ -NMSSM consists of five neutralinos which are mixtures of the bino ( $\tilde{B}$ ), the wino ( $\tilde{W}_3^0$ ), two higgsinos ( $\tilde{H}_d^0, \tilde{H}_u^0$ ) and the singlino ( $\tilde{S}$ ). The real symmetric



( $5 \times 5$ ) neutralino mass-matrix,  $\mathcal{M}_0$ , in the basis  $\psi_0 \equiv \{\tilde{B}, \tilde{W}_3^0, \tilde{H}_d^0, \tilde{H}_u^0, \tilde{S}\}$ , is given by [26]

$$\mathcal{M}_0 = \begin{pmatrix} M_1 & 0 & -\frac{g_1 v_d}{\sqrt{2}} & \frac{g_1 v_u}{\sqrt{2}} & 0 \\ \dots & M_2 & \frac{g_2 v_d}{\sqrt{2}} & -\frac{g_2 v_u}{\sqrt{2}} & 0 \\ \dots & \dots & 0 & -\mu_{\text{eff}} & -\lambda v_u \\ \dots & \dots & \dots & 0 & -\lambda v_d \\ \dots & \dots & \dots & \dots & 2\kappa v_s \end{pmatrix}, \quad (2.16)$$

where  $M_{1,2}$  are the soft SUSY-breaking masses for the  $U_1$  and the  $SU(2)$  gauginos, i.e., the bino and the wino, respectively. The  $[5,5]$  element of  $\mathcal{M}_0$ , i.e.,  $2\kappa v_s \equiv m_{\tilde{S}}$ , is the singlino mass term. The matrix  $\mathcal{M}_0$  can be diagonalized by an orthogonal  $5 \times 5$  matrix, ‘ $N$ ’, i.e.,

$$N\mathcal{M}_0 N^T = \mathcal{M}_D = \text{diag}(m_{\chi_1^0}, m_{\chi_2^0}, m_{\chi_3^0}, m_{\chi_4^0}, m_{\chi_5^0}), \quad (2.17)$$

with growing  $m_{\chi_i^0}$  as ‘ $i$ ’ increases whereas the neutralino mass eigenstates,  $\chi_i^0$ , are given by

$$\chi_i^0 = N_{ij} \psi_j^0, \quad \text{with } i, j = 1, 2, \dots, 5. \quad (2.18)$$

As we set  $M_2$  large, the heaviest neutralino ( $\chi_5^0$ ) is a nearly pure wino with  $m_{\chi_5^0} \approx M_2$  and is practically decoupled for our purposes. The lightest neutralino ( $\chi_1^0$ ) can get to be the lightest of the SUSY particles and, while  $R$ -parity is conserved, such an  $R$ -parity odd state becomes stable and could turn out to be a potential candidate for the cold DM.

The chargino sectors of the MSSM and that of the  $Z_3$ -NMSSM are structurally identical but for  $\mu \rightarrow \mu_{\text{eff}}$  for the latter. Thus, the  $2 \times 2$  chargino mass-matrix,  $\mathcal{M}_C$ , in the gauge bases  $\psi^+ = \{-i\tilde{W}^+, \tilde{H}_u^+\}$  and  $\psi^- = \{-i\tilde{W}^-, \tilde{H}_d^-\}$ , is given by [26]

$$\mathcal{M}_C = \begin{pmatrix} M_2 & g_2 v_u \\ g_2 v_d & \mu_{\text{eff}} \end{pmatrix}. \quad (2.19)$$

It requires two  $2 \times 2$  unitary matrices ‘ $U$ ’ and ‘ $V$ ’ to diagonalize this asymmetric matrix,  $\mathcal{M}_C$  [32], i.e.,

$$U^* \mathcal{M}_C V^\dagger = \text{diag}(m_{\chi_1^\pm}, m_{\chi_2^\pm}), \quad \text{with } m_{\chi_1^\pm} < m_{\chi_2^\pm}. \quad (2.20)$$

With  $M_2$  being set large in this work,  $\chi_1^\pm$  is higgsino-like while the wino-like  $\chi_2^\pm$  is essentially decoupled from the phenomenology we discuss.

### 2.3 The top and bottom squark sector

The tree-level mass-squared matrices for the top and bottom squarks in the NMSSM, in the basis of the weak eigenstates  $\{\tilde{t}_L, \tilde{t}_R\}$  and  $\{\tilde{b}_L, \tilde{b}_R\}$ , is given by, respectively,

$$\mathcal{M}_i^2 = \begin{pmatrix} m_{\tilde{t}_L}^2 & m_t X_t^\dagger \\ m_t X_t & m_{\tilde{t}_R}^2 \end{pmatrix}, \quad (2.21)$$

and

$$\mathcal{M}_b^2 = \begin{pmatrix} m_{\tilde{b}_L}^2 & m_b X_b^\dagger \\ m_b X_b & m_{\tilde{b}_R}^2 \end{pmatrix}, \quad (2.22)$$

where  $m_{\tilde{t}_L}^2 = m_{\tilde{Q}_{3L}}^2 + y_t^2 v_u^2 + (v_u^2 - v_d^2) \left( \frac{g_1^2}{12} - \frac{g_2^2}{4} \right)$ ,  $m_{\tilde{t}_R}^2 = m_{\tilde{U}_{3R}}^2 + y_t^2 v_u^2 - (v_u^2 - v_d^2) \frac{g_1^2}{3}$ ,  $m_{\tilde{b}_L}^2 = m_{\tilde{Q}_{3L}}^2 + y_b^2 v_d^2 + (v_u^2 - v_d^2) \left( \frac{g_1^2}{12} + \frac{g_2^2}{4} \right)$ ,  $m_{\tilde{b}_R}^2 = m_{\tilde{D}_{3R}}^2 + y_b^2 v_d^2 + (v_u^2 - v_d^2) \frac{g_1^2}{6}$  with  $m_{\tilde{Q}_{3L}}$ ,  $m_{\tilde{U}_{3R}}$  and  $m_{\tilde{D}_{3R}}$  being the soft masses for the  $SU(2)$  doublet, the up-type and the down-type  $SU(2)$  singlet squarks from the third generation, respectively. The squark mass eigenstates,  $\tilde{f}_1$  and  $\tilde{f}_2$  ( $m_{\tilde{f}_1} < m_{\tilde{f}_2}$ ) where  $\tilde{f}$  stands for  $\tilde{t}$  or  $\tilde{b}$ , respectively, are found on diagonalizing the matrix  $\mathcal{M}_{\tilde{f}}^2$  of equation (2.21) using a unitary matrix  $\mathcal{R}_{\tilde{f}}$  given by

$$\mathcal{R}_{\tilde{f}} = \begin{pmatrix} \cos \theta_{\tilde{f}} & \sin \theta_{\tilde{f}} \\ -\sin \theta_{\tilde{f}} & \cos \theta_{\tilde{f}} \end{pmatrix}, \quad (2.23)$$

where  $\theta_{\tilde{f}}$  is the squark mixing angle given by

$$\sin 2\theta_{\tilde{f}} = \frac{2m_f X_f}{m_{\tilde{f}_2}^2 - m_{\tilde{f}_1}^2}, \quad X_f = A_{\tilde{f}} - \mu_{\text{eff}} r, \quad (2.24)$$

where  $r = \cot \beta (\tan \beta)$  for the stop (sbottom) sector. Note that, in this formalism,  $\tilde{f}_1 \equiv \tilde{f}_L (\tilde{f}_R)$  when  $\theta_{\tilde{f}} = 0 (\frac{\pi}{2})$ . One could expect a light bottom squark along with a light top squark close by in mass when  $m_{\tilde{Q}_3}$  is relatively small and both of them being dominantly left-handed type.

## 2.4 Interactions of the ewinos with $\tilde{t}_1$ , the Higgs and the gauge bosons

We are now all set to discuss briefly the interactions of various ewinos with  $\tilde{t}_1$  and with the pertinent Higgs and gauge bosons which determine the nature and the strengths of the cascades that  $\tilde{t}_1$  undergoes.

### 2.4.1 Interactions of the ewinos with $\tilde{t}_1$

Decays of pair-produced  $\tilde{t}_1$ -s to the ewinos ( $\chi_i^0$  ( $i \neq 5$ ) and  $\chi_1^\pm$ ) that are central to the present work are governed by the following Lagrangian pieces:

$$\mathcal{L}_{\tilde{t}_1 \bar{b} \chi_1^+} = \bar{b} \left( f_L^{\chi_1^+} P_L + f_R^{\chi_1^+} P_R \right) \chi_1^{+c} \tilde{t}_1 + \text{h.c.}, \quad (2.25a)$$

$$\mathcal{L}_{\tilde{t}_1 \bar{t} \chi_i^0} = \bar{t} \left( f_L^{\chi_i^0} P_L + f_R^{\chi_i^0} P_R \right) \chi_i^0 \tilde{t}_1 + \text{h.c.}, \quad (2.25b)$$

where  $P_{L,R} = \frac{1}{2} (1 \mp \gamma^5)$  are the familiar projection operators and the various coefficients appearing in these equations are given by

$$f_L^{\chi_1^+} = y_b U_{12}^* \cos \theta_{\tilde{t}}, \quad (2.26a)$$

$$f_R^{\chi_1^+} = -g_2 V_{11} \cos \theta_{\tilde{t}} + y_t V_{12} \sin \theta_{\tilde{t}}, \quad (2.26b)$$

$$f_L^{\chi_i^0} = - \left[ \frac{g_1}{3\sqrt{2}} N_{i1} + \frac{g_2}{\sqrt{2}} N_{i2} \right] \cos \theta_{\tilde{t}} - y_t N_{i4} \sin \theta_{\tilde{t}}, \quad (2.27a)$$

$$f_R^{\chi_i^0} = \frac{2\sqrt{2}}{3} g_1 N_{i1}^* \sin \theta_{\tilde{t}} - y_t N_{i4}^* \cos \theta_{\tilde{t}}, \quad (2.27b)$$

where  $y_{b(t)} = \sqrt{2}m_{b(t)}/v \cos(\sin)\beta$  is the bottom (top) quark Yukawa coupling. Note that as we set  $M_2$  large,  $V_{11}, U_{11}, N_{i2}$  ( $i \neq 5$ ) are minuscule and can safely be ignored in this work.

With these in mind, a brief discussion on the implications of equations 2.25, 2.26 and 2.27 is in order. The way  $\theta_{\tilde{t}}$  is defined (see above), interactions of  $\tilde{t}_1 \sim \tilde{t}_L$  ( $\tilde{t}_R$ ) with the ewinos are going to be  $\cos \theta_{\tilde{t}}$  ( $\sin \theta_{\tilde{t}}$ )-enhanced. Thus, for  $\tilde{t}_1 \sim \tilde{t}_L$ , the term  $y_t N_{i4}^* \cos \theta_{\tilde{t}}$ , driven by  $y_t$ , in equation 2.27b, would clearly dominate over the term driven by  $y_b$  in equation 2.26a (for sure, for low to moderate values of  $\tan \beta$ ) and over the first term in equation 2.27a while all other contributions could be ignored. Phenomenologically, this is expected to make the decay  $\tilde{t}_1(\sim \tilde{t}_L) \rightarrow \chi_{3,4}^0$  dominate over its decays to  $b\chi_1^\pm$  and  $t\chi_{1,2}^0$ . On the other hand, for  $\tilde{t}_1(\sim \tilde{t}_R)$ , all three  $\sin \theta_{\tilde{t}}$ -dependent terms in equations 2.26b, 2.27a and 2.27b might get comparable. Hence decays of  $\tilde{t}_1$  to all related modes could compete, albeit the one to  $b\chi_1^\pm$  might enjoy some edge due to a larger phase space available to it. These considerations are going to be crucial in our analysis and for what we present subsequently in section 5.

#### 2.4.2 Interactions of the ewinos with the Higgs and the gauge bosons

The pertinent interactions in the current category are comprised of the ones like  $\chi_i^0 - \chi_j^0 - \Phi/Z$  (with  $i, j \in \{1, 2, 3, 4\}$ ) where  $\Phi$  includes the neutral Higgs bosons of both  $CP$ -even ( $h_i$ , including  $h_{\text{SM}}$ ) and  $CP$ -odd ( $a_i$ ) kinds and the ones involving  $\chi_1^\pm - \chi_{1,2}^0 - W^\pm$ .

Given that the interactions involving a pair of neutralinos are crucial for the collider and the DM phenomenologies alike, we present those below in their general form [10]. Following the convention introduced in section 2.1, the generic such interaction involving a  $CP$ -even scalar,  $h_i$ , in the basis presented in equation (2.7), is given by

$$g_{h_i \chi_j^0 \chi_k^0} = \left[ \frac{\lambda}{\sqrt{2}} [E_{h_i \hat{h}} N_{j5} (N_{k3} \sin \beta + N_{k4} \cos \beta) + E_{h_i \hat{H}} N_{j5} (N_{k4} \sin \beta - N_{k3} \cos \beta) \right. \\ \left. + E_{h_i \hat{s}} (N_{j3} N_{k4} - \frac{\kappa}{\lambda} N_{j5} N_{k5}) \right] + \frac{1}{2} [g_1 N_{j1} - g_2 N_{j2}] [E_{h_i \hat{h}} (N_{k3} \cos \beta - N_{k4} \sin \beta) \\ + E_{h_i \hat{H}} (N_{k3} \sin \beta + N_{k4} \cos \beta)] + \left[ j \longleftrightarrow k \right], \quad (2.28)$$

while the same involving a  $CP$ -odd scalar,  $a_i$ , in the basis shown in equation (2.9), reads

$$g_{a_i \chi_j^0 \chi_k^0} = \left[ i \left( \frac{\lambda}{\sqrt{2}} [\mathcal{O}_{iA} N_{j5} (N_{k4} \sin \beta + N_{k3} \cos \beta) + \mathcal{O}_{iS_I} (N_{j3} N_{k4} - \frac{\kappa}{\lambda} N_{j5} N_{k5})] \right. \right. \\ \left. \left. - \frac{1}{2} [g_1 N_{j1} - g_2 N_{j2}] [\mathcal{O}_{iA} (N_{k3} \sin \beta - N_{k4} \cos \beta)] \right) \right] + \left[ j \longleftrightarrow k \right]. \quad (2.29)$$

Note that when  $M_2$  is taken to be very large, only  $j, k \in \{1, 2, 3, 4\}$  are relevant and  $N_{j2, k2} \sim 0$ .

On the other hand, the interactions of the  $Z$ -boson with a pair of neutralinos and those of the  $W^\pm$ -boson with a neutralino and a chargino are given, respectively, by

$$g_{Z\chi_i^0\chi_j^0} = \frac{g_2}{2\cos\theta_W} (N_{i3}N_{j3} - N_{i4}N_{j4}), \quad (2.30)$$

$$g_{W^\pm\chi_i^0\chi_j^\mp} \sim \frac{g_2}{\sqrt{2}} (N_{i4}V_{j2}P_L - N_{i3}U_{j2}P_R), \quad (2.31)$$

with  $U_{j1}, V_{j1} \sim 0$  as  $M_2$  goes large.

For both the scalar and the pseudoscalar interactions with the ewinos, two general observations can be made from equations 2.28 and 2.29 which are much relevant in the context of the present work. First, neutral doublet scalars interact with a pair of neutralinos via their higgsino and singlino contents the strengths of which go as ‘ $\lambda$ ’. In contrast, their singlet counterparts interact with a pair of neutralinos exclusively via the higgsino or the singlino contents in the latter. While the first type of interactions are driven by ‘ $\lambda$ ’, the latter is proportional to ‘ $\kappa$ ’. Second, such interactions that are driven by the gauge couplings (in particular,  $g_1$ , which only is relevant for the present work as we set winos to be rather massive) always look for the gaugino and the higgsino contents in the two neutralinos and involve only the doublet scalars.

As for the interactions of the  $Z$ -boson to a pair of neutralinos, equation 2.30 indicates that these depend only on the higgsino contents of the involved neutralinos. Similarly, the same among the  $W^\pm$ -boson and a neutralino and a chargino depend on the higgsino contents of the latter two (albeit only when the wino is set very heavy) as can be seen in equation 2.31.

Further, it is important to note that, in regard to decays of a heavier ewino to a much lighter one, both neutralinos can have reasonable higgsino contents only via mixings of higgsinos with other gaugino/singlino states. In the present work, we bank on such mixings with the singlino, which is again driven by ‘ $\lambda$ ’ in the  $Z_3$ -NMSSM. Hence decays of higgsino-dominated ewinos to a singlino-dominated one, either with an accompanying scalar (Higgs) or a gauge boson, would be enhanced for larger values of ‘ $\lambda$ ’ when these decay modes are expected to compete as well.

### 3 The motivated region of the $Z_3$ -NMSSM parameter space

The region of  $Z_3$ -NMSSM parameter space that we target for the present study is guided by several considerations pertaining to the phenomenology of the scenario at the LHC and that relates to the DM sector. These include the requirements of a reasonably light  $\tilde{t}_1$ , which has a substantial cross section for being pair-produced at the LHC, something that we exploit directly in this work and a spectrum of relatively light ewinos with a bino-dominated LSP which can be a viable DM candidate only when accompanied by not so heavy singlino- and higgsino-like states and light enough singlet-like scalar(s), all of which might escape searches at the LHC till date [10]. Moreover, as pointed out earlier, such a spectra of ewinos and singlet scalars can be further motivated [10] on cosmological grounds as these could facilitate a strong first-order electroweak phase transition (SFOEWPT) in the early Universe, thus

paving the way for a successful electroweak baryogenesis (EWBG). However, given that in this work, we are mainly interested in the signatures at the LHC, we do not carry out a dedicated analysis of the nature of the phase transitions.

It is interesting to note that the chance of having a light bino-dominated LSP (with its mass around tens of GeV) that is a viable DM candidate is enhanced in the  $Z_3$ -NMSSM [10] when the same is moderately tempered with singlino and higgsino admixtures. This certainly requires the relevant mass-parameters, i.e.,  $M_1$ ,  $m_{\tilde{S}}$  and  $\mu_{\text{eff}}$ , to lie close by and hence the physical masses of these states to be of comparable magnitudes. Even then, an optimal tempering is possible only for larger values of ‘ $\lambda$ ’ for which the required rate of DM annihilation is ensured such that it does not over-close the Universe.

However, such a tempering, in turn, would tend to enhance the DMDD spin-independent (DMDD-SI) rate to a level that is ruled out by experiments [33]. Interestingly enough, it has recently been pointed out [10] that an occurrence of a so-called coupling ‘blind spot’ ( $g_{h_{\text{SM}}\chi_1^0\chi_1^0} \sim 0$ ) could save the situation. For the kind of spectrum of ewinos (i.e.,  $m_{\chi_1^0(\tilde{B})} < m_{\chi_2^0(\tilde{S})} < m_{\chi_{3,4}^0(\tilde{H})} \approx m_{\chi_1^\pm(\tilde{H})}$ ) that we consider, this is realized generically if

$$\left(m_{\chi_1^0} + \frac{2\lambda^2 v^2}{m_{\tilde{S}} - m_{\chi_1^0}}\right) \frac{1}{\mu_{\text{eff}} \sin 2\beta} \simeq -1. \quad (3.1)$$

Note that for a vanishing ‘ $\lambda$ ’, one retrieves the well-known blind spot condition in the MSSM, i.e.,  $m_{\chi_1^0}/\mu_{\text{eff}} \approx -\sin 2\beta$ , which implies  $m_{\chi_1^0}$  and  $\mu_{\text{eff}}$  to have a relative sign between them. A closer inspection of equation 3.1 reveals that for a finite ‘ $\lambda$ ’, as is the case in the NMSSM, there is a further possibility of realizing a blind spot even when  $m_{\chi_1^0}$  and  $\mu_{\text{eff}}$  carry the same sign, only if there is a relative sign between  $\mu_{\text{eff}}$  and  $m_{\tilde{S}}$  (or ‘ $\kappa$ ’, for that matter). Incidentally, again a moderate to the large value of ‘ $\lambda$ ’ is required for the blind spot mechanism to work.

These prompt us to work with larger values of ‘ $\lambda$ ’. Such a choice has an immediate implication for  $m_{h_{\text{SM}}}$  as the latter could now be found in the right ballpark even when  $\tilde{t}_1$  is reasonably light [34–37] which, in turn, renders the scenario more ‘natural’ and hence, theoretically more attractive. To our advantage, this would boost the production of a  $\tilde{t}_1$ -pair at the LHC. In passing, we note that (as is well known) the chiral contents of  $\tilde{t}_1$  may also crucially determine its decays (see section 2.4.1), thus affecting the sensitivities in its search. We take this issue up in section 4.2.

Thus, we find that the multiple roles played by a relatively large ‘ $\lambda$ ’ could all work in tandem to our advantage. Note, further, that optimally low values of ‘ $\kappa$ ’ and  $\mu_{\text{eff}}$  are required to find the singlino-dominated NLSP close by in mass to the LSP to facilitate an optimal tempering of an otherwise bino-dominated LSP. Furthermore, the smaller the value of  $\mu_{\text{eff}}$  that we could arrange to accommodate in our scenario (which evades the stringent LHC constraints), the more attractive would be the scenario on the ‘naturalness’ ground.

In this work, a relatively large ‘ $\lambda$ ’ continues to play a favorable role in the collider domain as well. Given that for an enhanced ‘ $\lambda$ ’, the mixing among the higgsino and the singlino states gets to be appreciable, decays of the higgsino-dominated states to a singlino-dominated state are preferred over those to the bino-dominated LSP, i.e.,  $\text{BR}[\tilde{H} \rightarrow \tilde{S} h_{\text{SM}}/Z/W^\pm] >$

$\text{BR}[\tilde{H} \rightarrow \tilde{B} h_{\text{SM}}/Z/W^\pm]$ . Considerations of the altered decay patterns of the higgsino-like states,  $\chi_{3,4}^0$ , that the presence of such an intermediate  $\chi_2^0$  triggers, would inevitably relax the stringent lower bounds on the masses of the former that are obtained by the LHC experiments by analyzing the final states,  $3\ell + \cancel{E}_T$  [20, 22, 38, 39] and  $1\ell + 2b\text{-jets} + \cancel{E}_T$  [40, 41]. Along the line with what has been shown in an MSSM setup in reference [23], here also some strengthening of the lower bounds on the masses of the ewinos, which previously got relaxed in their direct searches when assuming their altered decay patterns, is envisaged when searched for in the cascades of top squark pairs. Moreover, given that the altered cascade patterns of the ewinos imply the same for the cascade-patterns of the top squark, the current lower bounds on its mass could also be relaxed. This is likely to offer an additional strengthening of the reach for the ewinos at the LHC beyond the nominal expectation because of a larger production rate of such a relatively light top squark (enjoying a relaxed lower bound on its mass). As a result, searches at the HL-LHC, in absence of a discovery, would extend the lower bounds on the respective masses in a maximal way. We explore this issue briefly at length in this work.

As for the Higgs-like scalars of the  $Z_3$ -NMSSM, we are particularly interested in the relatively light singlet-like ones among them (in particular,  $a_s$ ) and the observed SM(doublet)-like Higgs boson while we consider the MSSM-like Higgs bosons ( $A, H, H^\pm$ ) to be much heavier and, hence, essentially decoupled. The latter is realized by considering a large value of  $A_\lambda$ . In fact, given that we already require a not so heavy singlino-like state which is the NLSP ( $\chi_2^0 \sim m_{\tilde{g}}$ ), the singlet-like (neutral) scalars,  $h_s$  (with  $m_{h_s}^2 \sim m_{\tilde{g}}^2$ ; see equation 2.11) and  $a_s$  (with  $m_{a_s}^2 \sim A_\kappa m_{\tilde{g}}$ ; see equation 2.15) would only have masses in the same ballpark of  $m_{\tilde{g}}$ .

However, note that, by restricting  $A_\kappa$  to smaller values ( $A_\kappa < m_{\tilde{g}}$ ), one can find  $a_s$  to be pretty light and still passing existing experimental bounds when it is dominantly a singlet by nature, which is the case since  $m_A$  is taken to be large. Thus,  $a_s$  might turn out to be the lightest of the excitations that the scenario possesses. Even if that be not the case, there are some general possibilities with  $a_s$  that are of particular phenomenological significance in the context of our present work. First, for  $m_{a_s} \approx 2m_{\chi_1^0}$ ,  $a_s$  would provide an efficient (and hence, maybe, much sought after) funnel for the mutual-annihilation of the moderately-tempered DM particle. Second, even when this is not the case, we would like to ensure that  $a_s$  is light enough such that the decay  $\chi_2^0 \rightarrow \chi_1^0 a_s$  is kinematically allowed. This would present us with new possibilities of cascade decays of heavier neutralinos which are yet to be considered by the LHC experiments in their searches and hence, when considered, are likely to result in relaxed lower bounds on the masses of all the involved SUSY states. As for  $m_{h_s} \approx m_{\tilde{g}}$ , one just needs to ensure that it is not too small such that the contribution of  $h_s$  to the DMDD-SI rate does not result in a breach of its experimental upper bound on the latter.

Guided by the discussion above, in table 1 we indicate the extended region of the  $Z_3$ -NMSSM parameter space which would be interesting for our purpose. A corresponding graphical illustration of such a motivated region of the parameter space is presented in figure 2. There, the presentation takes into account various experimental constraints coming from the DM and the Higgs sectors and involves the three most crucial quantities,  $M_1$ ,  $2|\kappa|/\lambda$  and  $\mu_{\text{eff}}$ , that characterize the augmented ewino and the Higgs sectors of the  $Z_3$ -NMSSM.

Varying parameters	$\lambda$	$ \kappa $	$\tan \beta$	$ \mu_{\text{eff}} $ (TeV)	$ A_\lambda $ (TeV)	$ A_\kappa $ (GeV)	$ M_1 $ (GeV)	$ A_t $ (TeV)	$m_{\tilde{Q}_3, \tilde{U}_3}$ (TeV)
Ranges	0.5–0.7	$\leq 0.1$	1–20	$\leq 1$	$\leq 10$	$\leq 150$	$\leq 200$	$\leq 10$	0.1–6

**Table 1.** Ranges of various input model parameters considered in this work. The wino mass,  $M_2$ , is kept fixed at a value as high as 2.5 TeV.

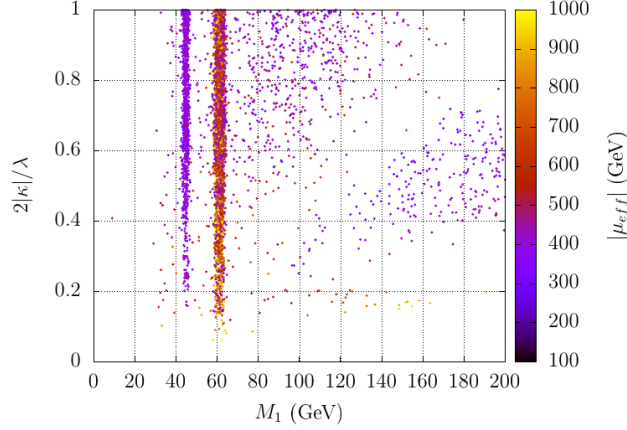


**Figure 2.** Scattered points in the  $M_1 - 2|\kappa|/\lambda$  plane that pass all relevant constraints from the DM and the Higgs sectors and those that are implemented in `NMSSMTools` (see section 4.1). Colors in the adjacent palette are representative of the magnitude of  $\mu_{\text{eff}}$  associated with each such point.

The criterion  $2|\kappa|/\lambda < 1$  ensures the NLSP to be singlino-like when we choose the LSP to be bino-like, i.e.,  $|M_1| < 2|\kappa|/\lambda$ . The two vertical bands correspond to the region of the parameter space where a pair of bino-like DM particles annihilate via  $Z$ -boson and  $h_{\text{SM}}$  funnels, respectively, whereas for all other points DM annihilation proceeds either through the  $a_s$ -funnel or via its co-annihilation with the singlino-like NLSP.<sup>2</sup> Note that, bino-like LSP mass  $\lesssim m_{h_{\text{SM}}}/4$  is barely allowed since a light scalar with mass  $\lesssim m_{h_{\text{SM}}}/2$ , which might act as a funnel, attracts stringent constraints from the studies of decays of the  $h_{\text{SM}}$  at the LHC. Furthermore, constraints coming from the DMDD sector (both SI and SD) and those from numerous searches of the ewinos at the LHC are continuously pushing  $\mu_{\text{eff}}$  upwards. In such a situation, the LHC might not be sensitive to this region of parameter space since the production cross-section of a pair of a relatively heavier higgsino becomes critically small. As discussed earlier, under such circumstances the larger production rate of a  $\tilde{t}_1$  pair at the LHC could enhance the reach for such ewinos which would appear in the cascade decays of  $\tilde{t}_1$ .

In section 5, we pick up a few representative (benchmark) scenarios out of the region of parameter space discussed above and study their implications for the LHC searches.

<sup>2</sup>The  $h_s$  funnel is generally not an efficient mode of DM annihilation as it is  $p$ -wave suppressed.



## 4 The setup of the analysis

In this section, we present the setup of our analysis. This includes a thorough description of various theoretical and experimental considerations ranging over the imposed constraints that are pertinent for the present work, the choice of the benchmark scenarios which are in sync with and are representative of the motivated region of the  $Z_3$ -NMSSM parameter space as outlined in section 3, motivating the NMSSM specific signals in those scenarios, a discussion of the relevant SM backgrounds and a brief mention of the approaches we took to optimize the signal strength with respect to the background. In the process, we also outline the computational tools we employ to carry out a state-of-the-art analysis as warranted by a phenomenological study of the present kind.

### 4.1 The spectra and the constraints

We rely on the package `NMSSMTools-v5.5.3` [42, 43] for generating the  $Z_3$ -NMSSM spectra. Viable spectra are required to be consistent with various known constraints, both of theoretical and experimental kinds, before those could be checked for their suitability for being called ‘benchmarks’ for our purpose. While `NMSSMTools` computes the masses, mixings and decays of various NMSSM excitations within the framework of  $Z_3$ -NMSSM, the built-in package `micrOMEGAs-v4.3` [44] provides us with the values of various key observables of the DM sector [45].

Furthermore, `NMSSMTools` ensures, on the theoretical side, that the spectra are free of tachyonic states, do not give rise to Landau poles in the evolution of various couplings and that the resulting scalar potentials do not have unphysical global minima. On the experimental side, it checks for the constraints from the flavor sector and a few primary ones from the LEP, Tevatron and the LHC. Among the latter set of constraints, the lower bounds arising from the LHC experiments on the masses of the lighter ewinos and  $\tilde{t}_1$  are particularly relevant for this work. In the context of the present study, the former restricts the masses of the higgsino-like ewinos (and hence  $\mu_{\text{eff}}$ ) from below. To keep our basic proposition and hence the analysis simple, we consider all the sfermions (including the sleptons), except for  $\tilde{t}_1$ , to be rather heavy (in the multi-TeV regime). Thus, those excitations are effectively decoupled from the phenomenology we discuss in this work. Thus, we make no attempt to reproduce the experimentally measured value of the anomalous muon magnetic moment ( $\mu_{g-2}$ ) [46, 47] which generically requires relatively light smuons in a SUSY scenario.

On the other hand, constraints on the Higgs sector coming from recent LHC studies are checked with the help of the dedicated packages like `HiggsBounds-v5.8.0` [48] and `HiggsSignals-v2.5.0` [49] which are interfaced with `NMSSMTools`. The mass of the (observed) SM-like Higgs boson is allowed to be in the range  $122 \text{ GeV} < m_{h_{\text{SM}}} < 128 \text{ GeV}$  to factor in the estimated theoretical uncertainties in its prediction.

As for the DM sector, in our conservative approach, we require the DM relic abundance ( $\Omega h^2$ ) to fall strictly within the band  $0.108 < \Omega h^2 < 0.132$ . This amounts to allowing for a theoretical uncertainty of 10% about the Planck-observed central value of 0.120 [50]. We also ensure compliance with various upper bounds on the rates of SI and SD DM scatterings off

the target nucleus of dedicated experiments some of which are incorporated in `NMSSMTools`. Note that, these DM constraints rule out smaller  $m_{h_S}$ , larger values of the coupling  $g_{h_{\text{SM}}\chi_1^0\chi_1^0}$  (mainly from DMDD-SI studies) and smaller values  $\mu_{\text{eff}}$  (mainly for DMDD-SD studies) [10, 28, 51–54].

## 4.2 The benchmark scenarios

In this section, we present four types of benchmark scenarios based broadly on the value of  $m_{\tilde{t}_1}$  while masses of the higgsino-like states ( $\sim \mu_{\text{eff}}$ ) for each such category are so chosen that the intended decays of  $\tilde{t}_1$  to the latter are kinematically allowed. Further, the phenomenology of top squarks is known to depend much on their ‘chiral’ contents. Hence we present the limiting situations with  $\tilde{t}_1 \approx \tilde{t}_L$  ( $\theta_{\tilde{t}} \sim 0$ ) and  $\tilde{t}_1 \approx \tilde{t}_R$  ( $\theta_{\tilde{t}} \sim \pi/2$ ), whenever warranted.

In table 2, we present five benchmark scenarios based on the above-mentioned criteria. The table contains, for each scenario, the input parameters that are varied, the relevant masses and mixings of various excitations, the branching fractions of the involved states decaying into some relevant ones along with the predicted values of some pertinent DM observables, such as the relic abundance and the DMDD-SI and DMDD-SD scattering rates.

Scenarios BP1 and BP2 have  $m_{\tilde{t}_1} \gtrsim 1$  TeV while  $\mu_{\text{eff}} \sim 650$  GeV. These values border on the reported lower bounds on the respective quantities from the LHC experiments, albeit somewhat naively. This is since, as has been pointed out already, the decay patterns of the involved states in our benchmark scenarios differ from what have been assumed by the experiments while deriving the said bounds.<sup>3</sup> These two scenarios differ in the chiral contents of  $\tilde{t}_1$ : while in BP1,  $\tilde{t}_1 \approx \tilde{t}_L$ , in BP2,  $\tilde{t}_1 \approx \tilde{t}_R$ . On the other hand, scenarios BP3 and BP4 are chosen with somewhat heavier  $\tilde{t}_1$  ( $m_{\tilde{t}_1} \sim 1.4 - 1.5$  TeV) and higgsino-like ewinos ( $\mu_{\text{eff}} \lesssim 950$  GeV) in mind. The lighter ewinos are also commensurately heavier in scenarios BP3 and BP4. These two points are chosen to demonstrate the sensitivity of the LHC to such more massive states in scenarios like ours. Here, the heavier such ewinos, which the LHC might find difficult to reach out to in their direct production modes, may still be produced in the decays of  $\tilde{t}_1$ . Note that when we move from scenarios BP1 and BP2 to BP3 and BP4, only those modifications made in the input parameters that involve the top squark sector and  $\mu_{\text{eff}}$  would have some practical phenomenological implications. Also, again, in BP3 (BP4),  $\tilde{t}_1 \approx \tilde{t}_L$  ( $\tilde{t}_R$ ).

It may be noted that the strongest possible lower bound on  $m_{\tilde{t}_1}$  ( $\gtrsim 1.2$  TeV) as reported by some of the recent LHC analyses [55] are based on a number of simplified assumptions (and that also, within the MSSM) which simply do not hold in specific but realistic scenarios like the one adopted in the present work wherein top squarks would undergo longer cascades by virtue of novel such ones of ewinos. Hence any such bound is expected to get relaxed. A systematic analysis of such a relaxation is beyond the scope of the present work and we reserve the same for a future investigation. However, with such a possibility in mind, we introduce one more scenario, BP5, with a comparatively small  $m_{\tilde{t}_1}$  ( $\approx 800$  GeV, with  $\tilde{t}_1 \simeq \tilde{t}_L$ ) which

---

<sup>3</sup>In that sense, we choose to remain conservative in the choice of these mass parameters and leave a quantitative estimation of the extent of possible relaxations of these bounds for a dedicated study.

Input/Observables	BP1	BP2	BP3	BP4	BP5
$\lambda$	0.588	0.588	0.689	0.689	0.662
$\kappa$	-0.052	-0.052	0.047	0.047	0.096
$\tan \beta$	8.63	8.63	7.83	7.83	6.35
$A_\lambda$ (GeV)	6146	6146	-7304	-7304	3112
$A_\kappa$ (GeV)	108.1	106.1	-16.5	-14.1	121.4
$\mu_{\text{eff}}$ (GeV)	645.5	645.5	-936.6	-936.6	452.4
$M_1$ (GeV)	32.2	31.8	62.5	61.5	-61.5
$M_{\tilde{Q}_3}$ (GeV)	600	5000	1100	6200	5300
$M_{\tilde{t}_R}$ (GeV)	5500	670	5500	1200	100
$A_t$ (GeV)	6242	6242	4506	4506	4369
$m_{\chi_1^0}$ (GeV)	31.9	31.6	61.9	60.9	-61.96
$m_{\chi_2^0}$ (GeV)	-108.5	-108.5	-131.6	-131.9	132.5
$m_{\chi_3^0}$ (GeV)	660.3	660.4	958.7	960.4	467.8
$m_{\chi_4^0}$ (GeV)	668.8	-668.9	-959.8	961.6	-470.2
$m_{\chi_5^0}$ (GeV)	2584.3	2586.7	2582.0	2587.4	2581.1
$m_{\chi_1^\pm}$ (GeV)	654.1	654.1	950.7	952.5	452.2
$m_{h_1} \equiv m_{h_{\text{SM}}}$ (GeV)	122.8	124.1	126.1	124.8	125.6
$m_{h_2}$ (GeV)	216.4	217.1	345.1	345.6	187.1
$m_{a_S}$ (GeV)	64.5	63.8	65.1	66.6	65.1
$m_{H^\pm}$ (GeV)	5739.5	5732.6	7386.1	7383.8	2911.5
$m_{\tilde{t}_1}$ (GeV)	1041.3 ( $\approx \tilde{t}_L$ )	1027.4 ( $\approx \tilde{t}_R$ )	1438.1 ( $\approx \tilde{t}_L$ )	1491.3 ( $\approx \tilde{t}_R$ )	802.3 ( $\approx \tilde{t}_R$ )
$\Delta m_1, \Delta m'_1$ (GeV)	$\sim 200, \sim 380$	$\sim 190, \sim 370$	$\sim 305, \sim 480$	$\sim 355, \sim 530$	$\sim 160, \sim 345$
$\Delta m_2, \Delta m'_2$ (GeV)	$\sim 430, \sim 465$	$\sim 430, \sim 465$	$\sim 700, \sim 745$	$\sim 700, \sim 740$	$\sim 212, \sim 240$
$\Omega h^2$	0.115	0.113	0.117	0.121	0.017
$\sigma_{\chi_1^0-p(n)}^{\text{SI}} \times 10^{47}$ (cm <sup>2</sup> )	0.16 (0.16)	0.13 (0.14)	1.56 (1.59)	1.62 (1.67)	1.7 (1.8)
$\sigma_{\chi_1^0-p(n)}^{\text{SD}} \times 10^{43}$ (cm <sup>2</sup> )	7.4 (-5.8)	7.4 (-5.8)	1.38 (-1.1)	1.37 (-1.1)	3.5 (-2.7)
$\sigma_{b\bar{b}}^{\text{IS}} \times 10^{31}$ (cm <sup>3</sup> /s)	13.5	1.0	13.1	11.4	0.2
$\sigma_{c\bar{c}}^{\text{IS}} \times 10^{31}$ (cm <sup>3</sup> /s)	0.03	0.05	0.3	0.5	0.01
$\sigma_{l\bar{l}, \{l=\mu^-, \tau^-\}}^{\text{IS}} \times 10^{31}$ (cm <sup>3</sup> /s)	1.2	0.15	1.3	1.6	0.02
$\text{BR}(\tilde{t}_1 \rightarrow \chi_1^0 t)$	0.04	0.2	0.03	0.2	0.15
$\text{BR}(\tilde{t}_1 \rightarrow \chi_2^0 t)$	0.07	0.03	0.05	0.02	0.05
$\text{BR}(\tilde{t}_1 \rightarrow \chi_3^0 t)$	0.45	0.18	0.45	0.19	0.17
$\text{BR}(\tilde{t}_1 \rightarrow \chi_4^0 t)$	0.42	0.16	0.45	0.18	0.17
$\text{BR}(\tilde{t}_1 \rightarrow \chi_1^\pm b)$	0.04	0.42	0.03	0.41	0.46
$\text{BR}(\chi_1^\pm \rightarrow \chi_1^0 W^\pm)$	0.15	0.15	0.12	0.12	0.14
$\text{BR}(\chi_1^\pm \rightarrow \chi_2^0 W^\pm)$	0.85	0.86	0.88	0.88	0.86
$\text{BR}(\chi_2^0 \rightarrow \chi_1^0 a_S)$	1	1	1	1	1
$\text{BR}(\chi_3^0 \rightarrow \chi_1^0 Z)$	0.1	0.1	0.07	0.08	0.05
$\text{BR}(\chi_3^0 \rightarrow \chi_1^0 h_{\text{SM}})$	0.056	0.056	0.04	0.04	0.07
$\text{BR}(\chi_3^0 \rightarrow \chi_2^0 Z)$	0.61	0.61	0.43	0.43	0.35
$\text{BR}(\chi_3^0 \rightarrow \chi_2^0 h_{\text{SM}})$	0.22	0.22	0.43	0.43	0.45
$\text{BR}(\chi_4^0 \rightarrow \chi_1^0 Z)$	0.06	0.06	0.04	0.04	0.1
$\text{BR}(\chi_4^0 \rightarrow \chi_1^0 h_{\text{SM}})$	0.09	0.09	0.08	0.08	0.03
$\text{BR}(\chi_4^0 \rightarrow \chi_2^0 Z)$	0.25	0.25	0.44	0.44	0.52
$\text{BR}(\chi_4^0 \rightarrow \chi_2^0 h_{\text{SM}})$	0.57	0.57	0.43	0.43	0.24
$\text{BR}(a_S \rightarrow b\bar{b})$	0.9	0.9	0.91	0.91	0.91

**Table 2.** Benchmark scenarios allowed by all relevant theoretical and experimental constraints (see text for details). Shown are the values of the pertinent input parameters defining the scenarios and the resulting masses, mass-splits, mixings, branching fractions of the relevant states along with the values of various DM observables.

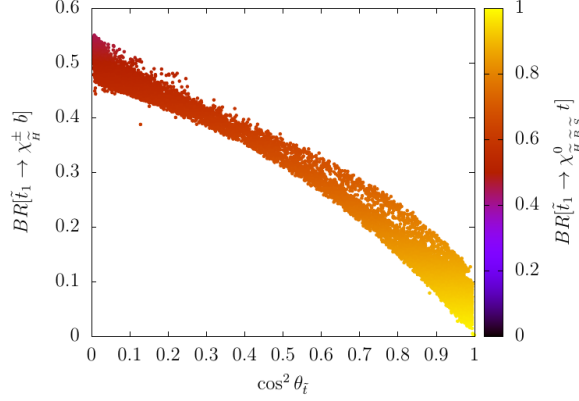


**Figure 3.** Variation of  $\text{BR}[\tilde{t}_1 \rightarrow \chi_{\tilde{H}}^\pm b]$  as a function of the mixing parameter of the stop sector, i.e.,  $\cos^2 \theta_{\tilde{t}}$ . The corresponding combined decay branching fraction of  $\tilde{t}_1$  to the lighter ewinos is shown via the palette.

might turn up lying just on the edge of exclusion in such a specific scenario under the same experimental analysis.

On the DM front, conformity with the Planck-observed relic abundance ( $\Omega h^2$ ) is ensured via mutual annihilation of the LSP DM via  $a_s$  ( $h_{\text{SM}}$ ) funnel in scenarios BP1, BP2 (BP3, BP4 and BP5). A compliance with the experimental upper bound on the DMDD-SI rate ( $\sigma^{\text{SI}}$ ) is achieved via the realization of a coupling ‘blind spot’ ( $g_{h_{\text{SM}}\chi_1^0\chi_1^0} \sim 0$ ), which is aided by having  $\kappa < 0$  ( $> 0$ ) when  $m_{\chi_1^0}$  and  $\mu_{\text{eff}}$  carry same (different) signs as are the cases in scenarios BP1 and BP3 (BP2, BP4 and BP5). These follow directly from the discussion of the blind spot condition of equation 3.1. As for the DMDD-SD rate ( $\sigma^{\text{SD}}$ ), it varies primarily as  $1/\mu_{\text{eff}}^4$  [10]. This is palpable in the values presented for  $\sigma_{\text{SD}}$  across the benchmark scenarios in table 2, all of which pass the latest experimental bound placed on it.

Turning to the relevant decays that shape the phenomenology at the LHC, one finds that, in all the benchmark scenarios,  $\tilde{t}_1$  decays dominantly to the higgsino-like states (albeit being heavier of the accessible ewinos) thanks to the large  $y_t$ -driven interactions. Thus, as discussed in section 2.4.1, for  $\tilde{t}_1 \approx \tilde{t}_L$  ( $\tilde{t}_R$ ), the decays  $\tilde{t}_1 \rightarrow t\chi_{3,4}^0$  ( $\tilde{t}_1 \rightarrow b\chi_1^\pm$ ) dominate, which is the case with scenarios BP1 and BP3 (BP2, BP4 and BP5). Such an observation is further in line with the general pattern of variations of the relevant decay branching fractions of  $\tilde{t}_1$  with the mixing parameter of the stop sector, i.e.,  $\cos^2 \theta_{\tilde{t}}$ , as resulted from our scan, which is illustrated in figure 3. Such a well-defined, falling (with  $\cos^2 \theta_{\tilde{t}}$ ) band has its origin in low to moderate  $\tan \beta \lesssim 20$  that we consider in our scan. In fact, for larger values of  $\tan \beta$  when  $y_b$  gets enhanced, we would expect large values of  $\text{BR}[\tilde{t}_1 \rightarrow \chi_{(\tilde{H})}^\pm b]$  (up to  $\sim 0.5$ ) even for large  $\cos^2 \theta_{\tilde{t}}$ , when  $\tilde{t}_1 \rightarrow \tilde{t}_L$ .

The size of the decay branching fractions of the ewinos to their lighter cousins, accompanied by a Higgs (scalar) or a gauge boson, following directly from the discussions in section 2.4.2. As noted there, the decays of the higgsino-like  $\chi_{3,4}^0, \chi_1^\pm$  to a singlino-dominated  $\chi_{2(\tilde{S})}^0$  or to a bino-dominated  $\chi_{1(\tilde{B})}^0$  depend on the higgsino admixtures in the latter states

and, for a larger ‘ $\lambda$ ’, these are larger for  $\chi_{2(\tilde{S})}^0$ . This is the reason why, in table 2, we find  $\chi_{3,4}^0$  dominantly decaying to  $\chi_2^0$  along with a  $Z$ -boson or a  $h_{\text{SM}}$ . Further, in scenarios BP1 and BP2, the observation that the decay of  $\chi_3^0$  dominantly yields  $Z$ -boson while that of  $\chi_4^0$  has a preference for  $h_{\text{SM}}$  is attributed to the so-called antipodal behavior of  $\chi_3^0$  and  $\chi_4^0$  [10, 56] in this regard. This effect is less dominant in scenarios BP3, BP4, and BP6 when  $\chi_{3,4}^0$  are much purer higgsino states given that larger values of  $\mu_{\text{eff}}$  in these scenarios result in smaller mixings among the higgsinos and the singlino. The scenario BP5 also shows cases of such an antipodal pattern in the decays of  $\chi_{3,4}^0$ , albeit the preferred modes of their decays get flipped when compared to scenarios BP1 and BP2. Also, note that the mass-splits between the singlino-dominated  $\chi_2^0$  and the bino-dominated  $\chi_1^0$  are such that  $\text{BR}[\chi_2^0 \rightarrow \chi_1^0 a_s] = 1$  for all the scenarios presented in table 2 and in all these cases  $a_s$  mostly decays to a  $b\bar{b}$  pair.

A pertinent observation at this point is that both  $h_{\text{SM}}$ , originating in the decays  $\chi_{3,4}^0 \rightarrow \chi_2^0 h_{\text{SM}}$ , and  $a_s$ , arising in the decay  $\chi_2^0 \rightarrow \chi_1^0 a_s$ , could be reasonably boosted. This can be understood in terms of various mass-splits among the states taking part in the cascade decays of  $\tilde{t}_1$  of which the following four, down the cascade, are relevant in our setup: (i)  $\Delta m_1 = m_{\tilde{t}_1} - (m_{\chi_{3,4}^0} + m_t)$ , (ii)  $\Delta m'_1 = m_{\tilde{t}_1} - (m_{\chi_1^\pm} + m_b)$  and (iii)  $\Delta m_2 = m_{\chi_{3,4}^0} - (m_{\chi_2^0} + m_{h_{\text{SM}}})$ , (iv)  $\Delta m'_2 = m_{\chi_1^\pm} - (m_{\chi_2^0} + m_W^\pm)$ . These sets of values are indicated for each of the benchmark scenarios in table 2. While  $\chi_2^0$  and  $h_{\text{SM}}$ , having similar masses, would share the overall boost available to them by virtue of the magnitude of  $\Delta m_2$ , the absolute boost acquired by  $h_{\text{SM}}$  would always be significant for a larger  $\Delta m_2$ , i.e., for larger  $m_{\chi_{3,4}^0} \sim \mu_{\text{eff}}$ . Nonetheless, the boost originally inherited by  $\chi_{3,4}^0$  from the decays  $\tilde{t}_1 \rightarrow \chi_{3,4}^0 t$  at the top of the cascade and which depends upon  $\Delta m_1$ , does percolate to some extent to  $h_{\text{SM}}$  downstream. Hence, for a fixed  $m_{\tilde{t}_1}$  and  $m_{\chi_2^0}$ , as  $m_{\chi_{3,4}^0}$  decreases (i.e.,  $\Delta m_1$  increases), the boost inherited by  $h_{\text{SM}}$  from the top of the cascade would likely increase at the cost of the boost it acquires immediately in the decays  $\chi_{3,4}^0 \rightarrow \chi_2^0 h_{\text{SM}}$  (as  $\Delta m_2$  decreases).

On the other hand,  $a_s$  is likely to derive most of its boost from that of  $\chi_2^0$  (and hence, again, the boost would mostly depend on  $\Delta m_2$ ) as it decays, thanks to the states participating in the decay  $\chi_2^0 \rightarrow \chi_1^0 a_s$  are all packed closely in mass at the bottom of the spectra. However, note that  $\chi_2^0$ , and hence  $a_s$ , arising from the cascade  $\tilde{t}_1 \rightarrow t \chi_{3,4}^0$ ,  $\chi_{3,4}^0 \rightarrow \chi_2^0 Z$  or from the cascade  $\tilde{t}_1 \rightarrow b \chi_1^\pm$ ,  $\chi_1^\pm \rightarrow \chi_2^0 W^\pm$  would be further boosted. This is primarily due to the fact that  $m_{Z/W^\pm} < m_{h_{\text{SM}}}$ , which has two implications for an enhanced boost for  $\chi_2^0$ . First, both  $\Delta m_2$  and  $\Delta m'_2$  are now larger thus resulting in larger overall boosts that would be available to the  $Z/W^\pm \chi_2^0$  final states (arising in the decays of  $\chi_{3,4}^0/\chi_1^\pm$ ) and (ii)  $\chi_2^0$  would now carry a bigger share of the available boost as compared to when it arises in association with  $h_{\text{SM}}$  in the decays of  $\chi_{3,4}^0$ .

In summary, in our benchmark scenarios,  $h_{\text{SM}}$  and  $a_s$  would be reasonably boosted because of much heavier  $\chi_{3,4}^0 \sim \mu_{\text{eff}}$  while  $m_{\chi_{1,2}^0} \sim M_1, m_{\tilde{S}}$  being on the lighter side. Hence the angular separations between the two  $b$ -jets originating from decays of  $h_{\text{SM}}/a_s$  would be on the smaller side, thus possibly giving rise to fat jets (which we call the ‘Higgs jets’) which could help identify such scalar states.

### 4.3 An NMSSM-specific signal and the SM backgrounds

A suitable NMSSM-specific signal under cascade decays of a pair-produced  $\tilde{t}_1$  in our target scenario could be figured out right from the decay patterns of  $\tilde{t}_1$  and the ewinos as illustrated in the Introduction. As indicated there,  $b$ -jets arising from the decays of the top quarks and various Higgs bosons ( $h_{\text{SM}}$  and  $a_s$ ) produced from the cascading  $\tilde{t}_1$  or from its direct decay to  $b\chi_1^\pm$ , which is predominant for  $\tilde{t}_1 \sim \tilde{t}_R$ , would dominate the signal final states. Note that the latter mode of decay of  $\tilde{t}_1$ , in which  $\chi_1^\pm$  appears in place of  $\chi_{3,4}^0$ , would subsequently miss out on an  $h_{\text{SM}}$  down the cascade in favour of a  $W^\pm$  boson.

In a rather busy final state that is thus expected under the circumstances, we lean heavily on an early tagging of the light NMSSM state  $a_s$  ( $m_{a_s} < m_Z$ ) by reconstructing the same in the peak of the invariant mass of a  $b$ -jet pair which it would decay dominantly to. In addition, tagging at least one  $h_{\text{SM}}$  at the invariant mass-peak of another  $b$ -jet pair would prove helpful in dealing with the background. Requiring an isolated lepton ( $e, \mu$ ) with its origin in the decay of a  $W^\pm$  (coming from the decay of a top quark or a  $\chi_1^\pm$  to which a  $\tilde{t}_1$  decays to at the top of the cascade) would help tame the mighty QCD background. As usual, the escaping LSPs would be the dominant contributors to  $\cancel{E}_T$  and an optimally strong lower cut on it is indispensable to suppress the SM background. Furthermore, in each event, there could be up to 6 additional  $b$ -jets that arise from decays of the top quarks and the untagged  $h_{\text{SM}}$  and  $a_s$  in the event. In addition, there will be a pair of light quark jets coming from the other  $W^\pm$  boson present in the event. Consequently, the final states will still be rather rich in jets (up to 8, at the parton level) even after the reconstruction of one each of  $a_s$  and  $h_{\text{SM}}$ . Thus, the signal we choose to study in this work is as follows:

$$1\ell(e, \mu) + (\geq 1) a_s(b\bar{b}) + (\geq 1) h_{\text{SM}}(b\bar{b}) + \geq 4 \text{ jets} + \cancel{E}_T. \quad (4.1)$$

Note that requiring at least one  $h_{\text{SM}}$  in the signal makes the latter draw contributions only from the cases where either one or both  $\tilde{t}_1$ 's decay to  $t\chi_{3,4}^0$ . In the first case, the other  $\tilde{t}_1$  would need to decay to  $b\chi_1^\pm$  for the purpose.

The dominant SM backgrounds for this final state arise from processes involving a  $t\bar{t}$  pair, viz.,

$$pp \rightarrow t\bar{t}, t\bar{t}h_{\text{SM}}, t\bar{t}b\bar{b}, t\bar{t}Z, t\bar{t}W^\pm, \quad (4.2)$$

where, the invariant mass of various pair-wise combinations of  $b$ -jets arising in the decays of the top quarks,  $Z$ -boson and  $h_{\text{SM}}$  might get reconstructed to  $m_{h_{\text{SM}}}$  and/or  $m_{a_s}$  thus faking the signal. On the other hand, possible backgrounds from processes like  $pp \rightarrow W^\pm + \text{jets}, Z + \text{jets}, h_{\text{SM}} + \text{jets}, W^\pm h_{\text{SM}}, Zh_{\text{SM}}, W^\pm Z$  are expected to be negligible [57, 58] when the signal contains so many hard jets alongside a hard lepton.

### 4.4 The simulation framework

Events for both the signal and the backgrounds are generated by considering up to two extra parton-level jets for each of the primary processes the primary processes contributing at the lowest order (LO) in the perturbation theory using **MadGraph5-aMC@NLO-v2.7.3** [59] for the 13 TeV LHC run. The default parton distribution function ('**nn231o1**' [60]) is employed with

a dynamic choice of the factorization scale given by  $Q^2 = \frac{1}{2} \sum_i M_i^{T^2} = \frac{1}{2} \sum_i (m_i^2 + p_{Ti}^2)$ , where  $M_i^T$  is the transverse mass of the ‘ $i$ ’-th final state particle. The primary process contributing to the signal is  $pp \rightarrow \tilde{t}_1 \tilde{t}_1^*$ , while for the backgrounds, those are the ones mentioned in equation 4.2. To generate the signal events **MadGraph5** is interfaced with the **NMSSM UFO** [61] model file as obtained from the package **FeynRules** [62].

Computations of the decay-kinematics of the unstable excitations and subsequent showering and hadronization are carried out using **PYTHIA8-v8.3** [63, 64] using the default **PYTHIA8** cards. As for the model-dependent masses and decay branching fractions of various **NMSSM** excitations, **PYTHIA8** reads those in from the **NMSSMTools**-generated **SLHA** [65] files linked to it for the purpose. We employ the **MLM** [66] approach, as implemented in **MadGraph5**, for the purpose of matching of partonic jets (from the LO matrix elements) to those coming from the parton showers. Finally, detector responses are taken into account using **DELPHES-v3.4.2** [67] running with the CMS detector card with some modifications in its lepton isolation criteria which are discussed in section 4.5.

Radiatively corrected cross section for the base process, i.e.,  $pp \rightarrow \tilde{t}_1 \tilde{t}_1^*$ , contributing to the signal is considered at the NLO+NLL level by employing a flat  $k$ -factor of 1.4 [68]. As for the base background processes, the  $k$ -factors considered are 1.4 [69], 1.2 [70], 1.8 [71], 1.35 [72], 1.5 [73] for the processes  $pp \rightarrow t\bar{t}$ ,  $t\bar{t}h_{\text{SM}}$ ,  $t\bar{t}b\bar{b}$ ,  $t\bar{t}Z$ ,  $t\bar{t}W^\pm$ , respectively.

#### 4.5 Object reconstruction

In this section, we describe how various composite observables are constructed out of the primary objects mentioned above, once the detector effects are considered via **DELPHES**.

- **Missing Transverse Energy (MET or  $\cancel{E}_T$ ):** The missing  $p_T$  vector is constructed out of the negative of the resultant  $p_T$  of all the visible entities in the detector and its magnitude is used as  $\cancel{E}_T$ .
- **Lepton ( $e, \mu$ ) selection:** Non-isolated electrons and muons are selected using the following  $p_T^{(\ell)}$  and (pseudo)rapidity ( $\eta_\ell$ ) cuts:

$$p_T^{(\ell)} > 30 \text{ GeV}, \quad |\eta_\ell| < 2.5, \quad \ell = e, \mu, \quad (4.3)$$

while mini-isolation [74] of each candidate lepton is ensured by demanding the combined  $p_T$  of all objects within a cone of radius  $r = 10/p_T^{(\ell)}$  about the candidate lepton is less than a certain fraction of the  $p_T$  carried by the same and hence imposing the condition

$$\frac{\sum p_T^{(\Delta R < r)}}{p_T^{(\ell)}} < I(\ell), \quad (4.4)$$

where  $\Delta R = \sqrt{\Delta_\phi^2 + \Delta_\eta^2}$ ,  $\Delta_\phi$  and  $\Delta_\eta$  being the angular distances from the candidate lepton in the azimuthal and the beam directions, respectively, and  $I(e, \mu) = (0.12, 0.25)$ .

- **Reconstructing the SM-like and the light (singlet-like) Higgs bosons:** As discussed earlier, due to their likely boosted nature, these Higgs bosons are reconstructed



as fat (Higgs) jets. The low-level energy flow (e-flow) objects, e.g., the tracks, the photons and the neutral hadrons are used as inputs to the package **Fastjet** [75]. Jets are then constructed using the Cambridge-Aachen (CA) algorithm with the radius parameter set to  $R = 1$  and by requiring  $p_T^{(j)} > 100$  GeV. The fat jets thus obtained are then treated with the mass drop tagger (MDT) [76, 77], with  $\mu = 0.67$  and  $y_{\text{cut}} > 0.09$ , to get rid of the  $b$ -jets from gluon splittings and the contamination from the underlying events (UE) while retaining the  $b$ -jets from the decays of the Higgs bosons and accompanying hard radiations off them [76]. The fat jets that pass MDT are referred to as tagged fat jets (FJ $_{b\bar{b}}$ ).

The two subjets unearthed during the first stage of declustering of each tagged fat jet are then matched with the  $b$ -quarks of a given event within a matching cone  $\Delta R = 0.3$ . When both subjets are found to be  $b$ -like, the covering fat jet is identified as either  $h_{\text{SM}}$  or  $a_s$  depending on whether  $m_{\text{FJ}(bb)} \in [100, 150]$  GeV or  $m_{\text{FJ}(bb)} \in [50, 80]$  GeV, the latter window being designed with the lighter Higgs boson in mind that has a mass of around 65 GeV for the benchmark scenarios we consider in this work.

- **Reconstructing the ordinary jets:** After reconstructing  $h_{\text{SM}}$  and  $a_s$ , the e-flow objects that are away from all the jets that constitute those Higgs bosons are clustered to form the ordinary jets using **Fastjet** and by employing the anti- $k_t$  algorithm, with the jet radius parameter  $R = 0.5$  and  $p_T^{(j)} > 20$  GeV. To identify such jets with possible residual  $b$ -jets in the event (for the signal, the ones from the top quark decays are there for sure), these are again matched with the  $b$ -quarks of the event.

## 5 Results

With the setup of our analysis now ben described, we move on to present our results. As mentioned earlier, two standard approaches are adopted to optimize the signal to background ratio, i.e., (i) the usual cut-based analysis (CBA) and (ii) the MVA using the BDT which learns and exploits the intrinsic kinematic features of the signal and the backgrounds (that may be essentially inaccessible to the CBA) thus aiding a more efficient discrimination of the signal from the background. It may be noted that LHC analyses triggering on a single lepton would include the kind of final state (equation 4.1) that has been considered in this work.

### 5.1 The cut-based analysis

The cut-based analysis, for our purpose, banks primarily on the following kinematic variables:

- $m_{\text{FJ}(bb)}$ , the invariant mass distribution of a pair of  $b$ -jets constituting a fat jet thanks to their large boosts when those originate in the decays of  $h_{\text{SM}}$  and/or  $a_s$ , as is the case for the signal final state,
- $m_T(p_T^{(\ell)}, \cancel{E}_T)$ , the transverse mass of a lepton- $\cancel{E}_T$  system, conventionally given by

$$m_T(p_T^{(\ell)}, \cancel{E}_T) = \sqrt{2 \times p_T^{(\ell)} \times \cancel{E}_T \times (1 - \cos \Delta\phi)} ,$$

where  $\Delta\phi$  is the opening angle between a charged lepton and the direction of  $\cancel{E}_T$  in the azimuthal plane. Given that  $\cancel{E}_T$  in a signal event is not directly correlated with the kinematics of the final-state lepton unlike in the case of background events where the leptons and the neutrinos, the sole carriers of  $\cancel{E}_T$  there at the parton level, both originate in the decays  $W^\pm \rightarrow \ell^\pm \nu_\ell$ , this variable is expected to serve as a good discriminator between the signal and the background events.

- The variable  $H_T^{(j)}$ , defined as the scalar sum of transverse momenta of all the jets (including the  $b$ -jets), i.e.,  $H_T^{(j)} = \sum_j |p_T^{(j)}|$ , is expected to peak at and extend to much higher values for the signal when compared to the background. This is since, for the former, the jets originate in the cascades of rather heavy SUSY states and, at the same time, the jet-multiplicity is much higher in our chosen signal final state than that is expected from the background. Note that, in our (cut-flow) study, only those jets that are left out after the reconstruction of  $h_{\text{SM}}$  and  $a_s$  concern  $H_T^{(j)}$ .
- The variable  $R_n$ , which is the ratio of the summed  $p_T$  of the leading ‘ $n$ ’ ‘ordinary’ jets and that involves all ‘ordinary’ jets in a given event and is given by [78]

$$R_n = \frac{\sum_{j=1}^n |p_T^{(j)}|}{H_T^{(j)}}.$$

Operationally, in this work, the ‘ordinary’ jets are comprised of all possible jets, including the  $b$ -jets that are left in an event after the reconstructions of  $h_{\text{SM}}$  and  $a_s$ . By construct,  $R_n = 1 (< 1)$  for the events with  $N_{\text{jet}} \leq n (> n)$ . Our choice of  $n = 3$ , i.e., of  $R_3$ , and a nontrivial lower cut on it, are guided by the fact that the signal final states in our scenario are expected to be characteristically rich in more than three rather hard jets, unlike in the case of the background.

- $\cancel{E}_T$ ; last but not the least, this variable, as is broadly the case in the search for physics beyond the SM with a new neutral, heavy, and stable excitation, remains to play the role of a crucial discriminator between a new physics signal and the SM background having typically large values for the former.

We now take a closer look at the differential distributions of both the signal and the background events in all these kinematic variables to decide over an optimal set of cuts on them that tends to maximize the signal significance over the background.

In figure 4(a) we present the invariant mass ( $m_{\text{FJ}(bb)}$ ) distributions of pairs of  $b$ -jets where the  $b$ -jets in each such pair are required to be found as a fat jet, for both the signal and the prominent backgrounds. Scenarios BP1 and BP2 are chosen as the representative ones for presenting the signal distributions. Three peaks are discernible in these distributions. The ones seen at around 65 GeV solely appear for the signal and indicate the presence of  $a_s (\rightarrow b\bar{b})$  in the event. The peak in the middle around  $m_Z$  comes from the background process  $pp \rightarrow t\bar{t}Z$  with the  $Z$ -boson decaying to a  $b\bar{b}$  pair. The peaks on the right occur

around  $m_{h_{\text{SM}}}$  and have their origins in the decays  $h_{\text{SM}} \rightarrow b\bar{b}$  in the signal where  $h_{\text{SM}}$  appears in the cascade decays of  $\tilde{t}_1$  and in the background from the process  $pp \rightarrow t\bar{t}h_{\text{SM}}$ . Relatively taller peaks at about  $m_{a_s}$  ( $\approx 65$  GeV) when compared to those about  $m_{h_{\text{SM}}}$  solely reflect larger yields of  $a_s$  than that of  $h_{\text{SM}}$  in the signal thanks to larger effective branching fractions in the former mode. It is found that, for the scenarios of our choice, requiring the events to lie in the window  $|m_{\text{FJ}(bb)} - m_{a_s}| < 15$  GeV picks up the signal events containing an  $a_s$  rather efficiently. Furthermore, selecting simultaneously the window  $|m_{\text{FJ}(bb)} - m_{h_{\text{SM}}}| < 25$  GeV helps significantly in getting rid of the background coming from the SM process  $pp \rightarrow t\bar{t}h_{\text{SM}}$ . Qualitatively, at the level of the  $m_{\text{FJ}(bb)}$  distributions, the overall situation does not change much in going from scenarios BP1 (BP2) to scenarios BP3 (BP4), respectively.

In figure 4(b) we present the differential distributions of the events in the variable  $m_T(p_T^{(\ell)}, \cancel{E}_T)$  for the same set of background processes as done for figure 4(a). It can be seen that for all the 1-lepton final states contributing to the background which arise from processes that include a  $t\bar{t}$  pair, the distributions of  $m_T(p_T^{(\ell)}, \cancel{E}_T)$  fall sharply beyond the (Jacobian) peaks about  $m_W$ . A visible departure (flattening) from such behavior over the tail, however, is observed for the process  $pp \rightarrow t\bar{t}Z$  which is to be attributed to the additional contributions to  $\cancel{E}_T$  coming from the decays  $Z \rightarrow \nu\bar{\nu}$  that are uncorrelated to the  $\ell\nu$ -system arising from  $W^\pm$ -boson decays. In general, for all the background processes, the extended tails in the  $m_T(p_T^{(\ell)}, \cancel{E}_T)$  distributions (instead of a more sharply dropping behavior, signifying an endpoint at  $m_W$ , as is theoretically expected) are to be attributed to the detector-induced smearing of momenta of various final state objects, which affects the estimation of  $\cancel{E}_T$  and hence  $m_T(p_T^{(\ell)}, \cancel{E}_T)$ . The accumulated effect becomes somewhat pronounced in the presence of more number of jets in the final state, as is the case with our signal. On the other hand, a similar lack of a strong correlation between the only lepton and  $\cancel{E}_T$  in the signal final state makes the corresponding  $m_T(p_T^{(\ell)}, \cancel{E}_T)$  distributions much too flatter. Further, those distributions extend to rather high values of  $m_T(p_T^{(\ell)}, \cancel{E}_T)$  as both the lepton and  $\cancel{E}_T$  in a signal event could get to be much harder. Guided by these distributions, we require  $m_T(p_T^{(\ell)}, \cancel{E}_T) \geq 100$  GeV to further optimize the signal to background ratio, once at least one each of  $h_{\text{SM}}$  and  $a_s$  are tagged.

Figure 4(c) illustrates the corresponding distributions for the variable  $H_T^{(j)}$ . As pointed out earlier, the peaks of the signal distributions shift to higher values when  $m_{\tilde{t}_1}$  increases and for the two benchmark scenarios these peaks are already well-separated from those for the background processes occurring at lower values of  $H_T^{(j)}$ . Given these, choosing  $H_T^{(j)} \geq 300$  GeV is found to be optimal for enhancing the signal to background ratio, once at least one each of  $h_{\text{SM}}$  and  $a_s$  are tagged.

As for the variable  $R_3$ , we impose a cut of  $R_3 < 0.85$  to maximize the signal significance. This implies that a  $p_T$ -sum amounting to more than 15% of  $H_T^{(j)}$  has to be carried by the jets in the events which are present beyond the three leading ones. As for a cut on  $\cancel{E}_T$ , we impose a moderately hard cut of  $\cancel{E}_T > 100$  GeV at the very outset. However, given that the variable  $m_T(p_T^{(\ell)}, \cancel{E}_T)$  is closely correlated to  $\cancel{E}_T$ , a subsequent lower cut on the former makes any further lower cut on the latter an overkill and hence unnecessary.

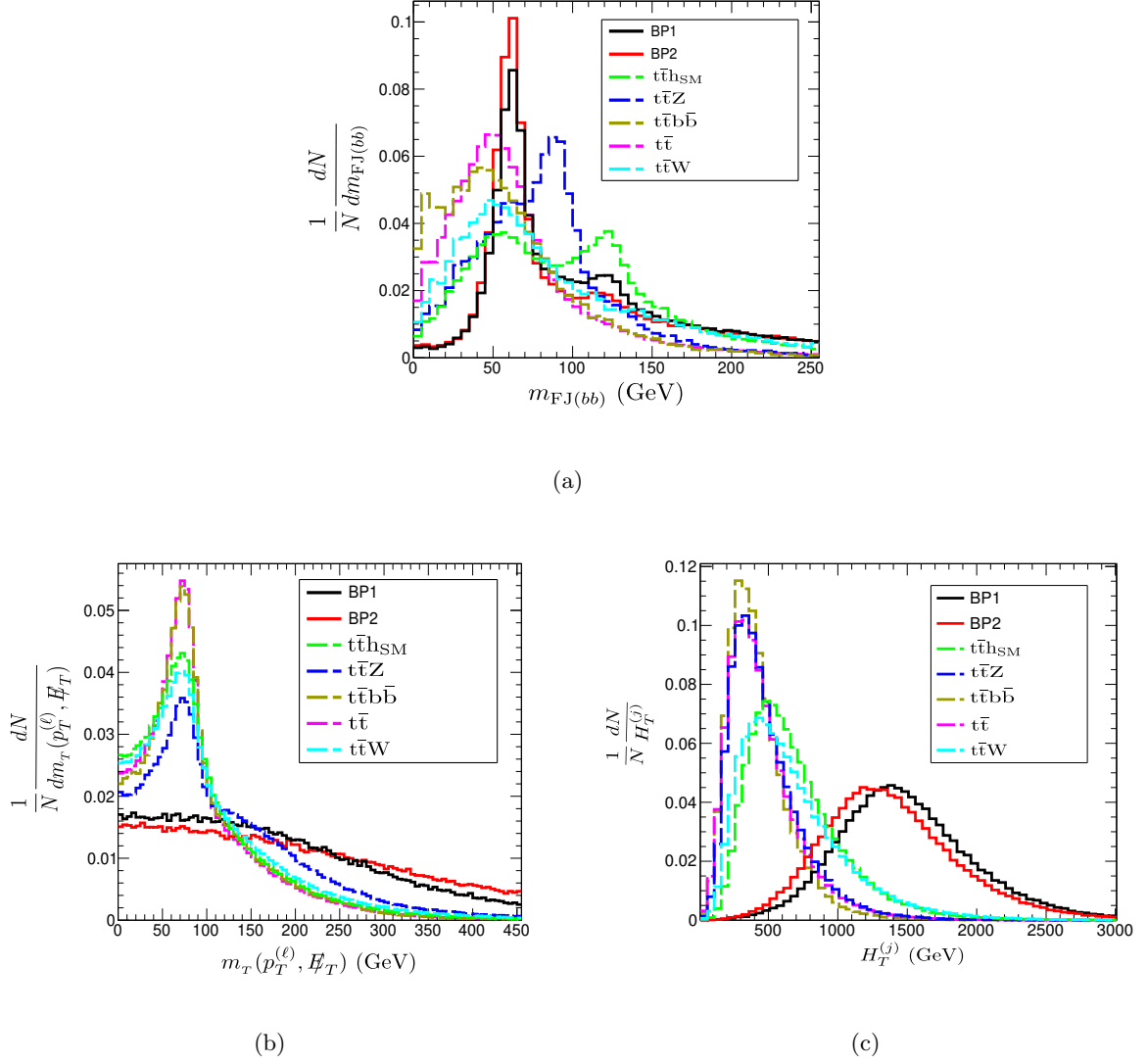


**Figure 4.** Normalised differential distributions of the number of events in the kinematic variables (a)  $m_{\text{FJ}(bb)}$ , (b)  $m_T(p_T^{(\ell)}, \cancel{E}_T)$  and (c)  $H_T^{(j)}$  for the backgrounds from various SM processes and for the signals in the benchmark scenarios BP1 and BP2.

In table 3 we present the cut-flow of the yields for our benchmark scenarios and for the primary SM background processes. The LO cross-sections of each of the processes, computed using **MadGraph** (with its default kinematic cuts), for the centre of mass energy of  $\sqrt{s} = 13$  TeV LHC are presented in the first column. The imposed cuts are what have been discussed earlier and are indicated in the top row of the table. These lead to the effective yields ( $\sigma_{eff}$ ), presented in the last column of the table. These are obtained by multiplying the fiducial cross-section  $\sigma_{\text{fid}}$  by the appropriate  $k$ -factors (as discussed in section 4.4) to take into account the higher-order corrections to the respective cross sections. It may be

Signal scenario	$\sigma$ (LO)	$\cancel{E}_T$ > 100 GeV	$n_\ell$ = 1	$n_{h_{\text{SM}}(b\bar{b})}$ $\geq 1$	$n_{a_S(b\bar{b})}$ $\geq 1$	$m_T(p_T^{(\ell)}, \cancel{E}_T)$ > 100 GeV	$H_T^{(j)}$ > 300 GeV	$R_3$ < 0.85	$\sigma_{\text{fid}}$ $\times k$
BP1	3.64	3.13	0.91	0.17	0.04	0.029	0.027	0.0219	0.0306
BP2	4.02	3.586	1.05	0.12	0.024	0.016	0.015	0.0103	0.0144
BP3	0.281	0.263	0.079	0.016	0.0046	0.0036	0.0035	0.0027	0.0038
BP4	0.202	0.192	0.0585	0.007	0.0017	0.0014	0.0012	0.0009	0.0013
BP5	21.86	18.42	5.16	0.54	0.068	0.049	0.042	0.031	0.0434
SMBG									
$t\bar{t}$	510000	36104.3	16373.1	62.4	0.29	0.166	0.104	0.0052	0.0073
$t\bar{t}h_{\text{SM}}$	405	46.13	22.32	1.25	0.013	0.0044	0.0015	0.0006	0.0007
$t\bar{t}Z$	590	67.2	32.91	0.4475	0.0068	0.0021	0.001	0.0005	0.0006
$t\bar{t}b\bar{b}$	13500	879.8	391.3	5.6	0.89	0.0068	–	–	–
$t\bar{t}W^\pm$	345	51.2	25.2	0.2	0.0006	0.0001	0.0001	–	–

**Table 3.** Values of the original, cut-flow (both at LO) and the fiducial (after folding in the appropriate  $k$ -factors) cross sections (in femtobarns) for various signal scenarios and for the primary SM background (SMBG) processes. The markings ‘–’ stand for cross-section values that are too small to be mentioned.

reiterated that requiring a significant  $\cancel{E}_T$  ( $> 100$  GeV) and a lepton in the events, at the very outset, would drastically suppress the large QCD background. However, the significant direct backgrounds from the processes involving a  $t\bar{t}$  pair, as can be gleaned from the entries in table 3, could be tamed rather effectively in our studies initially by requiring  $h_{\text{SM}}$  and  $a_S$  reconstructed and subsequently by putting cuts on  $m_T(p_T^{(\ell)}, \cancel{E}_T)$ ,  $H_T^{(j)}$  and  $R_3$ . It is seen that while the cuts on  $m_T(p_T^{(\ell)}, \cancel{E}_T)$ ,  $H_T^{(j)}$  affect the backgrounds moderately, the cut on  $R_3$  drastically eliminates them almost without hurting the signal.

Table 4 summarizes the signal significances  $\sigma = S/\sqrt{S+B}$ , where ‘ $S$ ’ and ‘ $B$ ’ correspond to the number of signal and the background events, respectively, after all the cuts are imposed, for all the benchmark scenarios and for integrated luminosity values of  $300 \text{ fb}^{-1}$  and  $3000 \text{ fb}^{-1}$  at the LHC. As can be seen, with  $\mathcal{L} = 300 \text{ fb}^{-1}$  at the LHC, even by exploiting the cascades of  $\tilde{t}_1$ , the lighter of the ewinos which the LHC would not be able to reach out to in their direct searches, cannot be even remotely probed. An integrated luminosity of  $3000 \text{ fb}^{-1}$ , for  $m_{\tilde{t}_1} \gtrsim 1 \text{ TeV}$ , as are the cases with scenarios BP1 and BP2, could scale (as  $\approx \sqrt{\mathcal{L}}$ ) the signal significance up above the coveted  $5\sigma$  level when one could expect to probe those lighter ewinos along with an NMSSM-specific lighter scalar in the cascade decays of  $\tilde{t}_1$ . However, for all other scenarios (like BP3 and BP4), with  $\tilde{t}_1$  moderately heavier than what they are in cases BP1 and BP2, the signal significance still remains abysmally small to be of any practical use, even for  $\mathcal{L} = 3000 \text{ fb}^{-1}$ . We further note that these signal sensitivities can get reduced by  $\sim 0.01\%$  if one considers a flat 10% uncertainty in the estimation of the SM background.

Integrated luminosity $\mathcal{L}$ (fb $^{-1}$ )	Signal significance $\sigma \left( = \frac{S}{\sqrt{S+B}} \right)$				
	BP1	BP2	BP3	BP4	BP5
300	2.7	2.0	0.6	0.2	3.3
3000	8.5	6.4	1.9	0.7	10.4

**Table 4.** Values of projected signal significances under a cut-based analysis for various benchmark scenarios and for two values of integrated luminosity at the 13 TeV LHC.

Note that, in the case of BP1 and BP3 where  $m_{\tilde{Q}_3}$  is not so large and the mixings between the ‘chiral’ partners in both the sbottom and the top squark sectors are small, both  $m_{\tilde{b}_1(\sim\tilde{b}_L)}$  and  $m_{\tilde{t}_1(\sim\tilde{t}_L)}$  would be on the smaller side and close by and hence their pair-production cross sections at the LHC would be of comparable strengths. Thus, given that the process  $pp \rightarrow \tilde{b}_1\tilde{b}_1^*$  could also yield the signal final state of our interest, the corresponding contribution to the same is also to be considered as well. However, this is expected to be suppressed given that  $\tilde{b}_1 \sim \tilde{b}_L$  would undergo the dominant decay  $\tilde{b}_1 \rightarrow t\chi_1^\pm$  (with branching ratio  $\sim 95\%$ ) when  $\chi_1^\pm$  is higgsino-like which would not lead to an SM Higgs boson, that we require in our signal, further down the cascade. Nonetheless, there will still be some residual contributions in the signal region we propose that could come from decaying  $W^\pm$ -bosons arising in the cascades of the top quarks and the lighter chargino. Our simulations for the benchmark points BP1 and BP3 show that the sensitivity of the proposed signal can be increased by up to about 25% when compared to the case where, as presented in Table 4, contributions from only  $pp \rightarrow \tilde{t}_1\tilde{t}_1^*$  are considered.

## 5.2 A multivariate analysis

The cut-based approach presented in section 5.1 is found to be reasonably efficient in suppressing an otherwise large SM background. However, the signal rate itself being tiny, especially for larger  $m_{\tilde{t}_1}$ , the LHC experiments hardly become sensitive to the same, even with an integrated luminosity of 3000 fb $^{-1}$ . Looking for a more optimal set of cuts to mitigate the problem becomes increasingly difficult when these are to be chosen solely based on intuition. A smarter set of cuts that segregates the signal events from the background ones in a more efficient manner would thus inevitably refer to complex kinematic entities, which are something that an MVA could essentially sniff out for us in the form of a single ‘discriminator’.

Towards this, the formalism of BDT (the so-called gradient boosting technique [24], to be precise) that we use within the MVA framework creates different disjoint decision trees by optimizing the cuts on various kinematic variables used for training the BDT and then applying them to subsets of events with different signal purities. If a signal event is wrongly classified as a background one or vice versa, it ‘boosts’ that event by increasing the corresponding weight and initiates a fresh tree with the new weight. Repeating this process optimizes the performance of the BDT till it finds the coveted discriminator. We use the package Toolkit for Multi Variate Analysis (TMVA) [24, 79], built-in in the CERN ROOT [80] analysis framework, for this purpose.

We note that though we have some representative values of  $m_{a_S}$  for our benchmark scenarios, this is an unknown parameter from the experimental perspective. Hence, in the MVA, choosing a pre-selected mass window to unearth a possible light Higgs bosons can be seen as biasing the analysis to a specific signal region with a precise kinematic attribute. On the other hand, leptons and the SM Higgs boson are, by now, rather well-understood objects at the LHC. Thus, for the MVA, we move away from the restricted signal region of the cut-based analysis that is characterized by an  $m_{\text{FJ}(bb)}$  window about a representative  $m_{a_S}$  value and require only the following known objects in the final state while training the BDT:

- i. an isolated lepton, which can effectively suppress the QCD background,
- ii. an SM Higgs boson is reconstructed in an appropriate  $b\bar{b}$  pair within the invariant mass-window  $|m_{\text{FJ}(bb)} - m_{h_{\text{SM}}}| < 25$  GeV, as has been already specified in section 5.1 and
- iii. an accompanying  $\cancel{E}_T > 80$  GeV.

We take the mass window of a possible light Higgs boson jet as a free variable ( $m_{j_{bb}} \equiv m_{\text{FJ}(bb)}(\text{low}) < 90$  GeV) without any loss of generality.

Once the BDT finds out a suitable discriminator modulo a particular reference to the possible presence of a light Higgs boson like  $a_S$ ), we focus on the above mentioned region by putting a cut on the BDT discriminator. As is expected, the resulting sample would primarily contain signal-enriched events, but, depending on the signal purity, would also include some events from the background. We then look for a light Higgs boson in this filtered sample which is expected to show up as a peak in the  $m_{j_{bb}}$  distribution.

To train the BDT we use 60% of the events from each of the signal and the background samples, while the other 40% of the events in each category are deployed for the purpose of testing the performance of the BDT. To start with, a large number of kinematic variables are constructed from various low-level objects present in the signal final state. However, on learning from the ranking and correlations among these variables as reported in the MVA training output, this number is gradually brought down to 14. The list of input kinematic variables according to their rankings, that tell about their effectiveness in decreasing order, is presented in table 5 for the benchmark scenario BP1. Since the objects in the signal final state originate in the cascades of massive top squarks ( $m_{\tilde{t}_1} \sim 1$  TeV), events possessing a larger number of harder jets are predominant for the signal when compared to the ones from the background. Hence, as can be gleaned from table 5, variables sensitive to jet-multiplicity and hardness of jets generally receive higher rankings. Interestingly enough, one can find from table 5 that various isolation variables ( $\Delta R$ ) generally tend to become important when compared to some prominent variables used in the cut-based analysis. The relatively higher importance of  $\Delta R(\ell, \cancel{E}_T)$  and  $p_T^{(\ell)}$  have pushed  $m_T(p_T^{(\ell)}, \cancel{E}_T)$ , which has a good correlation with these two variables, lower down the ranking. Also, once we require an  $h_{\text{SM}}$  to be reconstructed in a  $b$ -jet pair, the dominant background from  $t\bar{t}$  production will get eliminated while there may still be a number of  $b$ -jets left in a signal event. This attaches a reasonable importance to the  $b$ -jet multiplicity ( $N_b$ ) in an event as a means to



Rankings	Variables	Descriptions
1	$\Delta R(\ell, \cancel{E}_T)$	$\Delta R$ between the lepton and $\cancel{E}_T$ in the azimuthal plane
2	$p_T^{(\ell)}$	$p_T$ of the lepton
3	$H_T^{(j)}$	Scalar sum of $p_T$ of all jets
4	$N_b$	Number of $b$ -jets
5	$m_{j_{bb}} \equiv m_{\text{FJ}(bb)}(\text{low})$	Jet mass of the $bb$ fat jet with $m_{\text{FJ}(bb)} < 90$ GeV
6	$\Delta R(\ell, h_{\text{SM}})$	$\Delta R$ between the lepton and $h_{\text{SM}}$ in the azimuthal plane
7	$\Delta R(h_{\text{SM}}, \cancel{E}_T)$	$\Delta R$ between $h_{\text{SM}}$ and $\cancel{E}_T$
8	$p_T^{(h_{\text{SM}})}$	$p_T$ of $h_{\text{SM}}$
9	$m_T(p_T^{(\ell)}, \cancel{E}_T)$	Transverse mass of the system containing the lepton and $\cancel{E}_T$
10	$\cancel{E}_T$	Missing transverse energy in an event
11	$R_3$	The variable ‘ $R_{n=3}$ ’, as defined in section 5.1
12	$\Delta R(j_1, \cancel{E}_T)$	$\Delta R$ between the leading jet and $\cancel{E}_T$
13	$N_{\text{jet}}$	Number of ordinary jets
14	$\Delta R(\ell, j_1)$	$\Delta R$ between the lepton and the leading jet

**Table 5.** Rankings of various kinematic variables used for training the BDT in the scenario BP1.

filter out the signal. Note that, for all the benchmark scenarios, we have used the same set of kinematic variables as inputs to the MVA. This is in view of the fact that, although we have presented table 5 for scenario BP1, we find that the relative rankings of these kinematic variables remain grossly unaltered across the scenarios we are dealing with.

Finally, the signal significance for each scenario is evaluated by applying a cut to the BDT discriminator. For illustrative purposes, in the left (right) plot of figure 5, the yields in scenario BP1 (BP3) and those for the backgrounds are presented along with the signal significance as functions of the cut on the MVA output discriminator for an integrated luminosity of  $300 \text{ fb}^{-1}$ . The plot on the left indicates that a signal significance of  $\sim 1 - 6 \sigma$  can be obtained in scenario BP1 by choosing a lower cut of 0.9 on the MVA output discriminator which roughly translates to  $\sim 5 - 20 \sigma$  for an integrated luminosity of  $3000 \text{ fb}^{-1}$ . No essential changes in the features are noted for the benchmark scenario BP3 except for a general drop in the signal significance, as can be gleaned from the right plot of figure 5.

The projected values of signal significance for all the benchmark scenarios are presented in table 6 corresponding to accumulated luminosities of  $300 \text{ fb}^{-1}$  and  $3000 \text{ fb}^{-1}$ . It is to be noted that a two to three-fold enhancement in the signal significance is observed when using the MVA as compared to the cut-based approach. This can be attributed to the fact that a multi-dimensional treatment of the kinematic cuts by taking the correlations among the kinematic variables into account helps MVA arrive at a robust set of selection criteria almost without affecting the signal strength. In contrast, in the cut-based approach, many

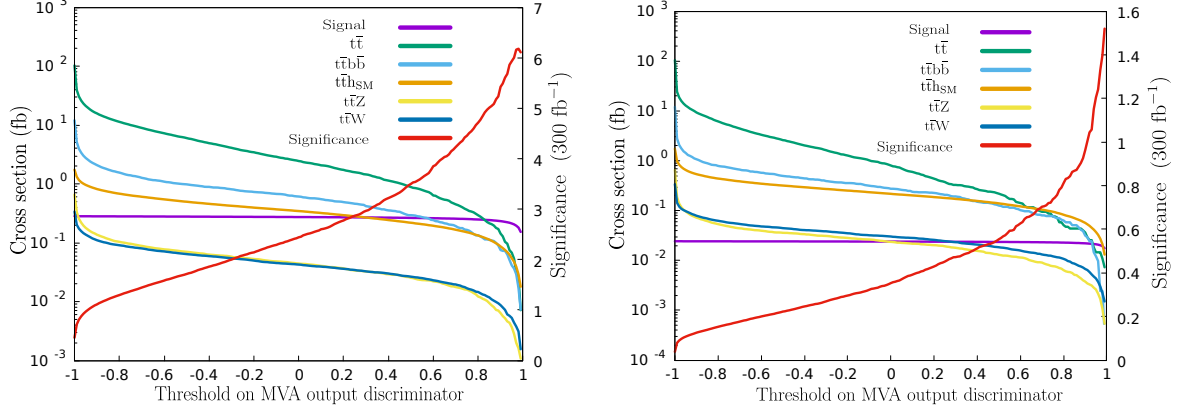


**Figure 5.** Distributions of the MVA output discriminators for the signal and the backgrounds along with the signal significances corresponding to an integrated luminosity of  $300 \text{ fb}^{-1}$  for the benchmark scenario BP1 (left) and BP3 (right).

Integrated luminosity $\mathcal{L} \text{ (fb}^{-1}\text{)}$	Signal significance $\sigma \left( = \frac{S}{\sqrt{S+B}} \right)$				
	BP1	BP2	BP3	BP4	BP5
300	5.5	4.5	1.2	0.7	9
3000	17	14	4	2.2	28

**Table 6.** Values of projected signal significance under MVA for various benchmark scenarios and for two values of integrated luminosity at the 13 TeV LHC.

of the variables remain practically unused in order to retain an optimal number of detectable signal events for a given value of accumulated luminosity. A reasonable signal significance of up to  $\sim 6\sigma$  is now seen to be achieved in scenario BP1 for an accumulated luminosity of  $300 \text{ fb}^{-1}$  while, for scenario BP3, the significance still remains sub-optimal at the level of  $\sim 1.5\sigma$ . The signal significance is expected to increase further by a factor of around 3 for an accumulated luminosity of  $3000 \text{ fb}^{-1}$ , as the same scales roughly as  $\sqrt{\mathcal{L}}$ .

A peak in the  $m_{j_{bb}}$  distribution would indicate the presence of a light Higgs boson of a possible NMSSM origin could now be searched for in the event sample. In figure 6, the combined distribution of  $m_{j_{bb}}$  is plotted with the event-sample that survives a cut of 0.9 on the BDT discriminator for the scenario BP1. The clear peak around  $m_{j_{bb}} = 65 \text{ GeV}$  confirms the presence of a light Higgs boson resonance in the signal region uncovered by the MVA. Note that the information on the mass of a light Higgs boson has nowhere been directly used in this analysis. Thus, the approach should work for any other scenario with a different assumption on  $m_{a_S}$  and would be able to find a low mass peak in the data in case such a resonance is present.

Before we end this section, the following general observations on the projected signal significance, based on a few benchmark scenarios that we consider, can be made:

- The cut-based analysis never delivers a signal significance close to the coveted  $5\sigma$  level

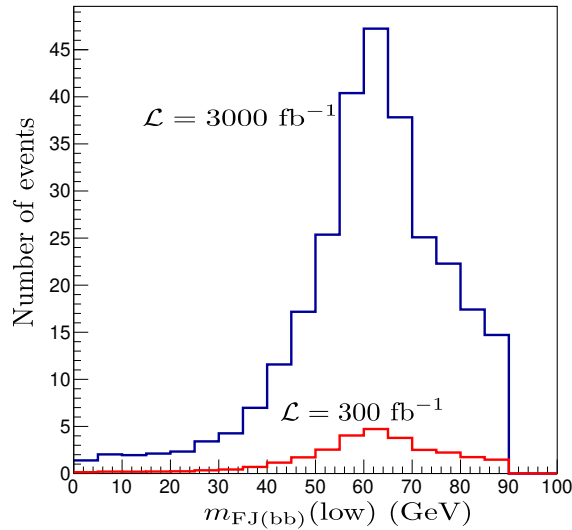


**Figure 6.** Differential distribution of the number of events in  $m_{\text{FJ}(bb)}(\text{low})$  for scenario BP1 with integrated luminosities of  $300 \text{ fb}^{-1}$  and  $3000 \text{ fb}^{-1}$  and with a cut on the BDT discriminator of 0.9 while keeping events in which at least one fat jet containing a pair of  $b$ 's appears.

with  $300 \text{ fb}^{-1}$  worth of LHC data.

- Hardly ever a  $5\sigma$  significance could be expected with  $\{m_{\tilde{t}_1}, \mu_{\text{eff}}\} \approx \{1.5 \text{ TeV}, 900 \text{ GeV}\}$ , even by employing an MVA and, that also, with data worth  $3000 \text{ fb}^{-1}$ .
- With  $3000 \text{ fb}^{-1}$  of data, one could expect an  $\sim 8\sigma$  ( $\sim 6\sigma$ ) signal significance for  $\tilde{t}_1 \approx \tilde{t}_L(\tilde{t}_R)$  and for  $\{m_{\tilde{t}_1}, \mu_{\text{eff}}\} \approx \{1 \text{ TeV}, 650 \text{ GeV}\}$  which drops sharply as  $m_{\tilde{t}_1}$  and  $\mu_{\text{eff}}$  increase.
- An MVA could deliver a  $\gtrsim 5\sigma$  signal significance for  $\{m_{\tilde{t}_1}, \mu_{\text{eff}}\} \approx \{1 \text{ TeV}, 650 \text{ GeV}\}$ , irrespective of the chiral content of  $\tilde{t}_1$ , even with  $300 \text{ fb}^{-1}$  of LHC data, something that can be seen as a rather meaningful improvement over what a cut-based analysis could offer with the same volume of data.

## 6 Summary and outlook

Searches for relatively light ewinos and a top squark have remained to be two priority programmes at the LHC, as these are intimately connected to the so-called ‘naturalness’ of a SUSY scenario. Stringent lower bounds that the LHC experiments have set on their masses are often based on some simplified theoretical assumptions. Even though due regard is to be paid to these emerging constraints which might be carrying a general message, departures from those simplistic assumptions are known to affect (relax) the reported bounds, sometimes drastically, resulting in the possibility that some such new physics excitations might have already popped up but are missed by the experiments. In this work, we exploit some such

possibilities that are characteristics of a scenario like the popular  $Z_3$ -NMSSM and are able to relax the reported lower bounds on the masses of both the lighter ewinos and  $\tilde{t}_1$ . We then demonstrate to what extent such ewinos could further be accessible in the cascade decays of  $\tilde{t}_1$ 's, produced in pairs at the LHC, when the masses of the ewinos in context exceed the (relaxed) bounds obtained by reinterpreting the results on their direct searches at the LHC.

The specific  $Z_3$ -NMSSM scenario that we adopt possesses a bino-like LSP and a singlet-like scalar, both lighter than 100 GeV, along with a singlino-like NLSP with its mass not much above 100 GeV. A pair of immediately heavier neutralinos and the lighter chargino are all higgsino-like with masses around or below  $\sim 1$  TeV (down to  $\sim 500$  GeV) while the heaviest neutralino and the heavier chargino are all wino-like and are taken to be rather massive such that those are practically decoupled from the physics we are interested in. The interesting region of the parameter space, in terms of the quantities like  $M_1$ ,  $\mu_{\text{eff}}$ ,  $m_{\tilde{g}}$ ,  $\lambda$ , is such that these conspire to give rise to a new blind spot (discussed recently in the literature) which leaves the DMDD-SI rate below its current experimental upper bound. On the other hand, the singlet-like scalar offers an annihilation funnel for a bino-like DM pair thus rendering the relic abundance in the right ballpark, as suggested by relevant experiments.

In addition to being a scenario which is much motivated as it may still offer a bino-like DM (unlike in the MSSM) satisfying all current constraints, it has the ingredients to trigger SFOEWPT in the early Universe thus setting the stage for the coveted EWBG. The relatively light singlet-like scalar serves as a crucial excitation for the scenario to work and its presence affects the collider phenomenology in an essential way resulting in altered LHC bounds on the masses of the ewinos and the lighter top squark. In the process, the scenario offers new signatures to search for at the LHC in the cascade decays of  $\tilde{t}_1$ 's via which hunt for the lighter of the ewinos could get extended beyond their direct LHC reaches.

The signal final state we study originates in the cascade decays of a pair of  $\tilde{t}_1$  that involve the two higgsino-dominated neutralinos,  $\chi_{3,4}^0$ , the singlino-dominated NLSP,  $\chi_2^0$ , and the singlet-like scalar,  $a_s$ , and is comprised of the parton-level states that are encircled above and, thus, and is given by '1 lepton + 4  $b$ -jets +  $\geq 4$  jets +  $\cancel{E}_T$ ', where the four  $b$ -jets are required to be reconstructed into an  $h_{\text{SM}}$  and an  $a_s$ . The pair-produced  $\tilde{t}_1$ 's may both decay via the first cascade mode  $\chi_{3,4}^0$  or one of them could decay via  $\chi_1^\pm$ . As can be seen, such a signal final state is rich in jets, in particular, in  $b$ -jets, and the sources of the lone lepton and the ordinary jets are the  $W^\pm$  bosons appearing in the cascades. Further, both  $h_{\text{SM}}$  and  $a_s$  could be reasonably boosted because of large mass-gaps among  $\tilde{t}_1$  and the ewinos appearing in its cascades. Hence, in our analysis, we treat those  $b$ -jets as fat jets. To summarize, the optimal signal region that emerges from our analysis is characterized by 1 isolated lepton, at least one each of  $h_{\text{SM}}$  and  $a_s$ , at least four other hard jets, and a large  $\cancel{E}_T$ .

It is to be noted that the LHC-sensitivity of the proposed final state crucially depends on two decay branching fractions, viz.,  $\text{BR}[\chi_{3,4}^0 \rightarrow h_{\text{SM}}\chi_2^0]$ , which is required to dominate over  $\text{BR}[\chi_{3,4}^0 \rightarrow h_{\text{SM}}\chi_1^0]$ , and  $\text{BR}[\chi_2^0 \rightarrow \chi_1^0 a_s]$ , which should be large. The first requirement is ensured when ' $\lambda$ ' is on the larger side. Compliance with the second one can be achieved for an optimally small mass-split between  $\chi_2^0$  and  $\chi_1^0$  such that the only allowed two-body decay of  $\chi_2^0$  is  $\chi_2^0 \rightarrow \chi_1^0 a_s$ . That these simultaneous requirements happen to prefer the

region of the parameter space that facilitates an SFOEWPT and that such a scenario having a bino-dominated LSP nicely complies with the constraints from the DM and cosmology experiments, make the proposed signal all the more characteristic of such a scenario.

We have presented the comparative sensitivities of the 13 TeV LHC to the proposed signal (in terms of the signal significance) for accumulated luminosities of  $300 \text{ fb}^{-1}$  and  $3000 \text{ fb}^{-1}$  by referring to a few benchmark scenarios and by performing a usual cut-based analysis, followed by a multivariate one. The benchmark scenarios are broadly categorized by the masses and the chiral contents of  $\tilde{t}_1$ . While the experimental sensitivity to the signal has the expected inverse dependence on  $m_{\tilde{t}_1}$ , the same on the chiral content of  $\tilde{t}_1$  mounts from the fact that its effective branching fraction to  $h_{\text{SM}}$  is expected to be significantly larger for  $\tilde{t}_1 \approx \tilde{t}_L$ .

We find that, with data worth  $300 \text{ fb}^{-1}$ , a usual cut-based analysis would not be able to reach out to these ewinos in the cascades of a pair of top squarks produced directly at the LHC. Instead, an MVA can be sensitive to the higgsino-like ewinos with masses  $\gtrsim 650 \text{ GeV}$  when  $\tilde{t}_1$  is not much heavier than 1 TeV. On the other hand, with an accumulated luminosity of  $\sim 3000 \text{ fb}^{-1}$ , states as massive as the above ones can already be probed in a cut-based approach. However, even an MVA on such a data set is unlikely to find these ewinos when their masses approach a TeV and the  $m_{\tilde{t}_1}$  hits  $\sim 1.5 \text{ TeV}$ .

It can thus be concluded that with a larger volume of available LHC data and when aided by the power of the MVA, one should be able to probe significantly heavier higgsino-like ewinos (and hence, larger  $\mu_{\text{eff}}$ ) of the  $Z_3$ -NMSSM scenario at the  $\sim 13 \text{ TeV}$  LHC in the cascades of pair-produced  $\tilde{t}_1$ 's. However, such a possibility gets quickly restricted as  $m_{\tilde{t}_1}$  increases. Our present analysis tends to indicate that a limiting  $5\sigma$  reach, under the most favorable of the setups discussed in this work, could perhaps only be achieved for  $m_{\tilde{t}_1}, \mu_{\text{eff}} \lesssim 1.3 \text{ TeV}, 1 \text{ TeV}$ . Applications of deep-learning methods might be an obvious way forward to extend the reach in these masses.

Nonetheless, the signal we study remains to be rather typical to a spectrum discussed in this work which is both motivated and consolidated from multiple theoretical and experimental considerations. Hence, once observed, a signal like this could promptly point back to such a spectrum that includes a relatively light ewino and a light scalar, both having a singlet origin, along with a little heavier higgsino-like ewinos and not so heavy a top squark. It may, however, be noted that a flipped hierarchy between the bino- and the singlino-like states (i.e., the LSP (NLSP) is singlino (bino)-dominated) relative to the scenario we discuss in this work, could also lead to a similar final state at the LHC if ' $\lambda$ ' is on the smaller side when  $\text{BR}[\chi_{3,4}^0 \rightarrow h_{\text{SM}}\chi_2^0]$  would again dominate over  $\text{BR}[\chi_{3,4}^0 \rightarrow h_{\text{SM}}\chi_1^0]$ . However, examining the viability of such a scenario in detail in the present context and then looking for a resolution of a possible ambiguity that it could give rise to are beyond the scope of the present study.

## 7 Acknowledgments

SR is supported by the funding available from the Department of Atomic Energy (DAE), Government of India for the Regional Centre for Accelerator-based Particle Physics (RCAPP) at Harish-Chandra Research Institute (HRI). SR is also supported by the Infosys

award for excellence in research through HRI. SR would like to thank MG and the Department of High Energy Physics, Tata Institute of Fundamental Research, Mumbai, India for hosting him during the course of this collaborative work. SR further acknowledges the use of the High-performance Scientific Computing facility and RECAPP's cluster computing facility at HRI and thanks Chandan Kanaujiya and Ravindra Yadav for their technical assistance at these facilities.

## References

- [1] J. E. Kim and H. P. Nilles, Phys. Lett. B **138** (1984), 150-154 doi:10.1016/0370-2693(84)91890-2
- [2] G. Aad *et al.* [ATLAS], Phys. Lett. B **716** (2012), 1-29 doi:10.1016/j.physletb.2012.08.020 [arXiv:1207.7214 [hep-ex]].
- [3] S. Chatrchyan *et al.* [CMS], Phys. Lett. B **716** (2012), 30-61 doi:10.1016/j.physletb.2012.08.021 [arXiv:1207.7235 [hep-ex]].
- [4] J. Beuria and A. Datta, JHEP **11** (2017), 042 doi:10.1007/JHEP11(2017)042 [arXiv:1705.08208 [hep-ph]].
- [5] J. Beuria, U. Chattopadhyay, A. Datta and A. Dey, JHEP **04** (2017), 024 doi:10.1007/JHEP04(2017)024 [arXiv:1612.06803 [hep-ph]].
- [6] S. Baum, M. Carena, N. R. Shah, C. E. M. Wagner and Y. Wang, JHEP **03** (2021), 055 doi:10.1007/JHEP03(2021)055 [arXiv:2009.10743 [hep-ph]].
- [7] P. Athron, C. Balazs, A. Fowlie, G. Pozzo, G. White and Y. Zhang, JHEP **11** (2019), 151 doi:10.1007/JHEP11(2019)151 [arXiv:1908.11847 [hep-ph]].
- [8] A. Chatterjee, A. Datta and S. Roy, JHEP **06** (2022), 108 doi:10.1007/JHEP06(2022)108 [arXiv:2202.12476 [hep-ph]].
- [9] S. Akula, C. Balázs, L. Dunn and G. White, JHEP **11** (2017), 051 doi:10.1007/JHEP11(2017)051 [arXiv:1706.09898 [hep-ph]].
- [10] W. Abdallah, A. Datta and S. Roy, JHEP **04** (2021), 122 doi:10.1007/JHEP04(2021)122 [arXiv:2012.04026 [hep-ph]].
- [11] U. Ellwanger and A. M. Teixeira, JHEP **10** (2014), 113 doi:10.1007/JHEP10(2014)113 [arXiv:1406.7221 [hep-ph]].
- [12] U. Ellwanger, JHEP **02** (2017), 051 doi:10.1007/JHEP02(2017)051 [arXiv:1612.06574 [hep-ph]].
- [13] U. Ellwanger and C. Hugonie, Eur. Phys. J. C **78** (2018) no.9, 735 doi:10.1140/epjc/s10052-018-6204-3 [arXiv:1806.09478 [hep-ph]].
- [14] W. Abdallah, A. Chatterjee and A. Datta, JHEP **09** (2019), 095 doi:10.1007/JHEP09(2019)095 [arXiv:1907.06270 [hep-ph]].
- [15] M. Guchait and A. Roy, Phys. Rev. D **102** (2020) no.7, 075023 doi:10.1103/PhysRevD.102.075023 [arXiv:2005.05190 [hep-ph]].
- [16] R. K. Barman, G. Bélanger, B. Bhattacharjee, R. Godbole, D. Sengupta and X. Tata, Phys. Rev. D **103** (2021) no.1, 015029 doi:10.1103/PhysRevD.103.015029 [arXiv:2006.07854 [hep-ph]].

- [17] A. M. Sirunyan *et al.* [CMS], JHEP **03** (2018), 166 doi:10.1007/JHEP03(2018)166 [arXiv:1709.05406 [hep-ex]].
- [18] M. Aaboud *et al.* [ATLAS], Eur. Phys. J. C **78** (2018) no.12, 995 doi:10.1140/epjc/s10052-018-6423-7 [arXiv:1803.02762 [hep-ex]].
- [19] M. Aaboud *et al.* [ATLAS], Phys. Rev. D **98** (2018) no.9, 092012 doi:10.1103/PhysRevD.98.092012 [arXiv:1806.02293 [hep-ex]].
- [20] G. Aad *et al.* [ATLAS], Phys. Rev. D **101** (2020) no.7, 072001 doi:10.1103/PhysRevD.101.072001 [arXiv:1912.08479 [hep-ex]].
- [21] [ATLAS], ATLAS-CONF-2020-015.
- [22] A. M. Sirunyan *et al.* [CMS], JHEP **03** (2018), 160 doi:10.1007/JHEP03(2018)160 [arXiv:1801.03957 [hep-ex]].
- [23] M. Guchait, A. Roy and S. Sharma, Phys. Rev. D **104** (2021) no.5, 055032 doi:10.1103/PhysRevD.104.055032 [arXiv:2103.09810 [hep-ph]].
- [24] A. Hocker, P. Speckmayer, J. Stelzer, J. Therhaag, E. von Toerne, H. Voss, M. Backes, T. Carli, O. Cohen and A. Christov, *et al.* [arXiv:physics/0703039 [physics.data-an]].
- [25] J. H. Friedman, Comput. Stat. Data Anal. **38** (2002), 367-378 doi:10.1016/S0167-9473(01)00065-2
- [26] U. Ellwanger, C. Hugonie and A. M. Teixeira, Phys. Rept. **496** (2010), 1-77 doi:10.1016/j.physrep.2010.07.001 [arXiv:0910.1785 [hep-ph]].
- [27] D. J. Miller, R. Nevzorov and P. M. Zerwas, Nucl. Phys. B **681** (2004), 3-30 doi:10.1016/j.nuclphysb.2003.12.021 [arXiv:hep-ph/0304049 [hep-ph]].
- [28] M. Badziak, M. Olechowski and P. Szczerbiak, JHEP **03** (2016), 179 doi:10.1007/JHEP03(2016)179 [arXiv:1512.02472 [hep-ph]].
- [29] U. Ellwanger, Eur. Phys. J. C **71** (2011), 1782 doi:10.1140/epjc/s10052-011-1782-3 [arXiv:1108.0157 [hep-ph]].
- [30] H. E. Haber, R. Hempfling and A. H. Hoang, Z. Phys. C **75** (1997), 539-554 doi:10.1007/s002880050498 [arXiv:hep-ph/9609331 [hep-ph]].
- [31] A. Djouadi, Phys. Rept. **459** (2008), 1-241 doi:10.1016/j.physrep.2007.10.005 [arXiv:hep-ph/0503173 [hep-ph]].
- [32] J. F. Gunion and H. E. Haber, Nucl. Phys. B **272** (1986), 1 [erratum: Nucl. Phys. B **402** (1993), 567-569] doi:10.1016/0550-3213(86)90340-8
- [33] S. Baum, M. Carena, N. R. Shah and C. E. M. Wagner, JHEP **04** (2018), 069 doi:10.1007/JHEP04(2018)069 [arXiv:1712.09873 [hep-ph]].
- [34] J. R. Ellis, K. Enqvist, D. V. Nanopoulos and F. Zwirner, Mod. Phys. Lett. A **1** (1986), 57 doi:10.1142/S0217732386000105
- [35] R. Barbieri and G. F. Giudice, Nucl. Phys. B **306** (1988), 63-76 doi:10.1016/0550-3213(88)90171-X
- [36] H. Baer, V. Barger, P. Huang, A. Mustafayev and X. Tata, Phys. Rev. Lett. **109** (2012), 161802 doi:10.1103/PhysRevLett.109.161802 [arXiv:1207.3343 [hep-ph]].



- [37] H. Baer, V. Barger, P. Huang, D. Mickelson, A. Mustafayev and X. Tata, Phys. Rev. D **87** (2013) no.11, 115028 doi:10.1103/PhysRevD.87.115028 [arXiv:1212.2655 [hep-ph]].
- [38] G. Aad *et al.* [ATLAS], Eur. Phys. J. C **81** (2021) no.12, 1118 doi:10.1140/epjc/s10052-021-09749-7 [arXiv:2106.01676 [hep-ex]].
- [39] A. Tumasyan *et al.* [CMS], JHEP **04** (2022), 147 doi:10.1007/JHEP04(2022)147 [arXiv:2106.14246 [hep-ex]].
- [40] G. Aad *et al.* [ATLAS], Eur. Phys. J. C **80** (2020) no.8, 691 doi:10.1140/epjc/s10052-020-8050-3 [arXiv:1909.09226 [hep-ex]].
- [41] A. M. Sirunyan *et al.* [CMS], JHEP **11** (2017), 029 doi:10.1007/JHEP11(2017)029 [arXiv:1706.09933 [hep-ex]].
- [42] U. Ellwanger and C. Hugonie, Comput. Phys. Commun. **175** (2006), 290-303 doi:10.1016/j.cpc.2006.04.004 [arXiv:hep-ph/0508022 [hep-ph]].
- [43] D. Das, U. Ellwanger and A. M. Teixeira, Comput. Phys. Commun. **183** (2012), 774-779 doi:10.1016/j.cpc.2011.11.021 [arXiv:1106.5633 [hep-ph]].
- [44] G. Belanger, F. Boudjema, A. Pukhov and A. Semenov, Comput. Phys. Commun. **176** (2007), 367-382 doi:10.1016/j.cpc.2006.11.008 [arXiv:hep-ph/0607059 [hep-ph]].
- [45] M. Abdughani, Y. Z. Fan, C. T. Lu, T. P. Tang and Y. L. S. Tsai, JHEP **07** (2022), 127 doi:10.1007/JHEP07(2022)127 [arXiv:2111.02946 [astro-ph.HE]].
- [46] B. Abi *et al.* [Muon g-2], Phys. Rev. Lett. **126** (2021) no.14, 141801 doi:10.1103/PhysRevLett.126.141801 [arXiv:2104.03281 [hep-ex]].
- [47] G. W. Bennett *et al.* [Muon g-2], Phys. Rev. D **73** (2006), 072003 doi:10.1103/PhysRevD.73.072003 [arXiv:hep-ex/0602035 [hep-ex]].
- [48] P. Bechtle, D. Dercks, S. Heinemeyer, T. Klingl, T. Stefaniak, G. Weiglein and J. Wittbrodt, Eur. Phys. J. C **80** (2020) no.12, 1211 doi:10.1140/epjc/s10052-020-08557-9 [arXiv:2006.06007 [hep-ph]].
- [49] P. Bechtle, S. Heinemeyer, T. Klingl, T. Stefaniak, G. Weiglein and J. Wittbrodt, Eur. Phys. J. C **81** (2021) no.2, 145 doi:10.1140/epjc/s10052-021-08942-y [arXiv:2012.09197 [hep-ph]].
- [50] N. Aghanim *et al.* [Planck], Astron. Astrophys. **641** (2020), A6 [erratum: Astron. Astrophys. **652** (2021), C4] doi:10.1051/0004-6361/201833910 [arXiv:1807.06209 [astro-ph.CO]].
- [51] C. Cheung, L. J. Hall, D. Pinner and J. T. Ruderman, JHEP **05** (2013), 100 doi:10.1007/JHEP05(2013)100 [arXiv:1211.4873 [hep-ph]].
- [52] C. Cheung, M. Papucci, D. Sanford, N. R. Shah and K. M. Zurek, Phys. Rev. D **90** (2014) no.7, 075011 doi:10.1103/PhysRevD.90.075011 [arXiv:1406.6372 [hep-ph]].
- [53] M. Badziak, M. Olechowski and P. Szczerbiak, PoS **PLANCK2015** (2015), 130 [arXiv:1601.00768 [hep-ph]].
- [54] M. Badziak, M. Olechowski and P. Szczerbiak, JHEP **07** (2017), 050 doi:10.1007/JHEP07(2017)050 [arXiv:1705.00227 [hep-ph]].
- [55] G. Aad *et al.* [ATLAS], Eur. Phys. J. C **80** (2020) no.11, 1080 doi:10.1140/epjc/s10052-020-08469-8 [arXiv:2006.05880 [hep-ex]].

- [56] L. Calibbi, J. M. Lindert, T. Ota and Y. Takanishi, JHEP **11** (2014), 106 doi:10.1007/JHEP11(2014)106 [arXiv:1410.5730 [hep-ph]].
- [57] G. Aad *et al.* [ATLAS], Eur. Phys. J. C **83** (2023) no.7, 561 doi:10.1140/epjc/s10052-023-11543-6 [arXiv:2211.08028 [hep-ex]].
- [58] G. Aad *et al.* [ATLAS], Eur. Phys. J. C **81** (2021) no.7, 600 [erratum: Eur. Phys. J. C **81** (2021) no.10, 956] doi:10.1140/epjc/s10052-021-09748-8 [arXiv:2101.01629 [hep-ex]].
- [59] J. Alwall, R. Frederix, S. Frixione, V. Hirschi, F. Maltoni, O. Mattelaer, H. S. Shao, T. Stelzer, P. Torrielli and M. Zaro, JHEP **07** (2014), 079 doi:10.1007/JHEP07(2014)079 [arXiv:1405.0301 [hep-ph]].
- [60] R. D. Ball, L. Del Debbio, S. Forte, A. Guffanti, J. I. Latorre, J. Rojo and M. Ubiali, Nucl. Phys. B **838** (2010), 136-206 doi:10.1016/j.nuclphysb.2010.05.008 [arXiv:1002.4407 [hep-ph]].
- [61] C. Degrande, C. Duhr, B. Fuks, D. Grellscheid, O. Mattelaer and T. Reiter, Comput. Phys. Commun. **183** (2012), 1201-1214 doi:10.1016/j.cpc.2012.01.022 [arXiv:1108.2040 [hep-ph]].
- [62] A. Alloul, N. D. Christensen, C. Degrande, C. Duhr and B. Fuks, Comput. Phys. Commun. **185** (2014), 2250-2300 doi:10.1016/j.cpc.2014.04.012 [arXiv:1310.1921 [hep-ph]].
- [63] T. Sjostrand, S. Mrenna and P. Z. Skands, JHEP **05** (2006), 026 doi:10.1088/1126-6708/2006/05/026 [arXiv:hep-ph/0603175 [hep-ph]].
- [64] T. Sjostrand, S. Mrenna and P. Z. Skands, Comput. Phys. Commun. **178** (2008), 852-867 doi:10.1016/j.cpc.2008.01.036 [arXiv:0710.3820 [hep-ph]].
- [65] P. Z. Skands, B. C. Allanach, H. Baer, C. Balazs, G. Belanger, F. Boudjema, A. Djouadi, R. Godbole, J. Guasch and S. Heinemeyer, *et al.* JHEP **07** (2004), 036 doi:10.1088/1126-6708/2004/07/036 [arXiv:hep-ph/0311123 [hep-ph]].
- [66] M. L. Mangano, M. Moretti, F. Piccinini and M. Treccani, JHEP **01** (2007), 013 doi:10.1088/1126-6708/2007/01/013 [arXiv:hep-ph/0611129 [hep-ph]].
- [67] J. de Favereau *et al.* [DELPHES 3], JHEP **02** (2014), 057 doi:10.1007/JHEP02(2014)057 [arXiv:1307.6346 [hep-ex]].
- [68] A. Broggio, A. Ferroglia, M. Neubert, L. Vernazza and L. L. Yang, JHEP **07** (2013), 042 doi:10.1007/JHEP07(2013)042 [arXiv:1304.2411 [hep-ph]].
- [69] K. Melnikov and M. Schulze, JHEP **08** (2009), 049 doi:10.1088/1126-6708/2009/08/049 [arXiv:0907.3090 [hep-ph]].
- [70] W. Beenakker, S. Dittmaier, M. Kramer, B. Plumper, M. Spira and P. M. Zerwas, Nucl. Phys. B **653** (2003), 151-203 doi:10.1016/S0550-3213(03)00044-0 [arXiv:hep-ph/0211352 [hep-ph]].
- [71] F. Bucci, S. Kallweit, S. Pozzorini and M. F. Zoller, JHEP **12** (2019), 015 doi:10.1007/JHEP12(2019)015 [arXiv:1907.13624 [hep-ph]].
- [72] A. Kardos, Z. Trocsanyi and C. Papadopoulos, Phys. Rev. D **85** (2012), 054015 doi:10.1103/PhysRevD.85.054015 [arXiv:1111.0610 [hep-ph]].
- [73] S. von Buddenbrock, R. Ruiz and B. Mellado, Phys. Lett. B **811** (2020), 135964 doi:10.1016/j.physletb.2020.135964 [arXiv:2009.00032 [hep-ph]].
- [74] V. Khachatryan *et al.* [CMS], JHEP **08** (2016), 122 doi:10.1007/JHEP08(2016)122 [arXiv:1605.04608 [hep-ex]].

- [75] M. Cacciari, G. P. Salam and G. Soyez, Eur. Phys. J. C **72** (2012), 1896  
doi:10.1140/epjc/s10052-012-1896-2 [arXiv:1111.6097 [hep-ph]].
- [76] J. M. Butterworth, A. R. Davison, M. Rubin and G. P. Salam, Phys. Rev. Lett. **100** (2008), 242001 doi:10.1103/PhysRevLett.100.242001 [arXiv:0802.2470 [hep-ph]].
- [77] M. Dasgupta, A. Fregoso, S. Marzani and G. P. Salam, JHEP **09** (2013), 029  
doi:10.1007/JHEP09(2013)029 [arXiv:1307.0007 [hep-ph]].
- [78] M. Guchait and D. Sengupta, Phys. Rev. D **84** (2011), 055010  
doi:10.1103/PhysRevD.84.055010 [arXiv:1102.4785 [hep-ph]].
- [79] H. Voss, A. Hocker, J. Stelzer and F. Tegenfeldt, PoS **ACAT** (2007), 040  
doi:10.22323/1.050.0040
- [80] R. Brun and F. Rademakers, Nucl. Instrum. Meth. A **389** (1997), 81-86  
doi:10.1016/S0168-9002(97)00048-X